Muography
how - why- who/where/how

Cristina Cârloganu
LPC/IN2P3/ CNRS

Photon imaging

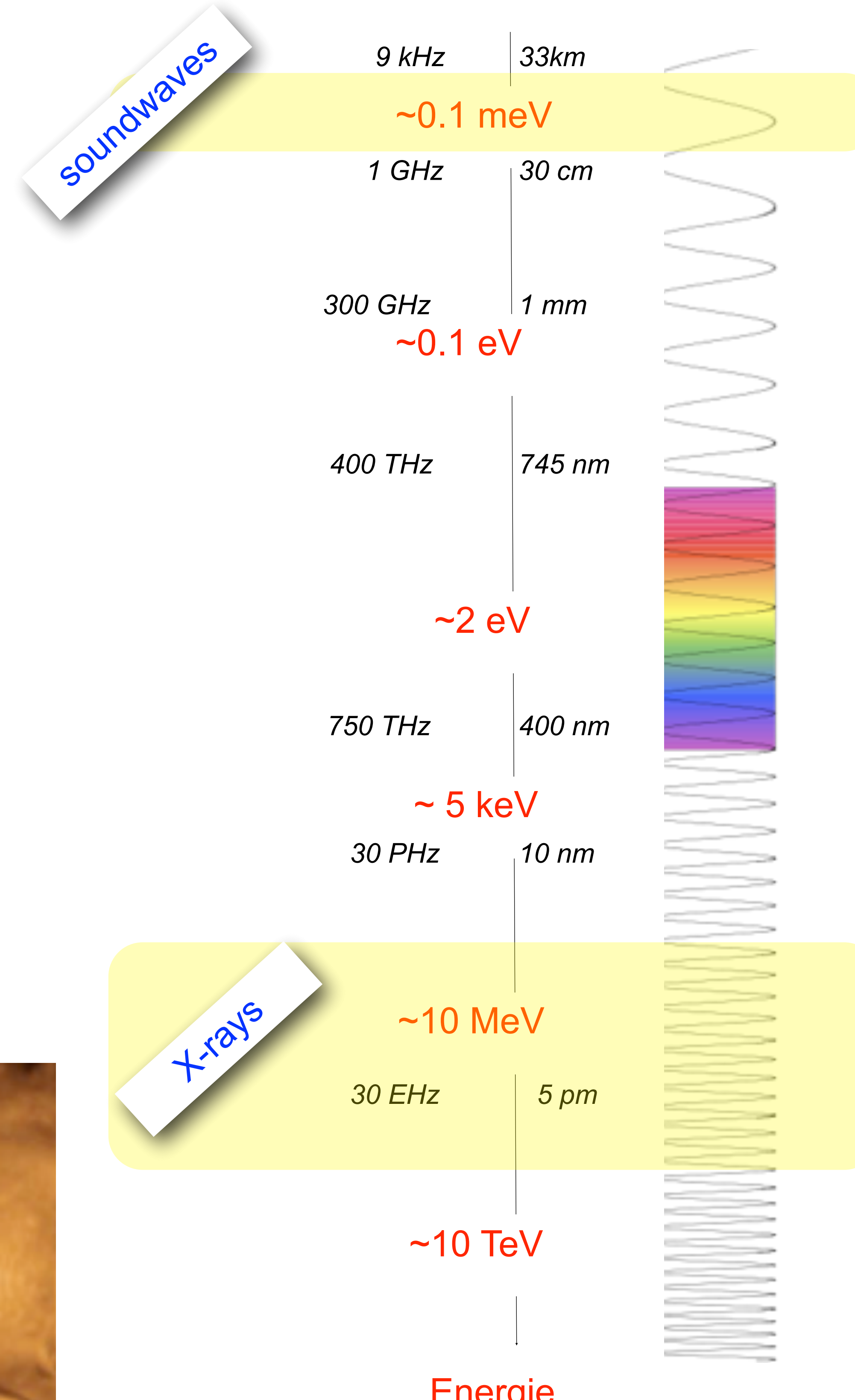

Photon imaging

RAdio Detection And Ranging

La Galaxie M87

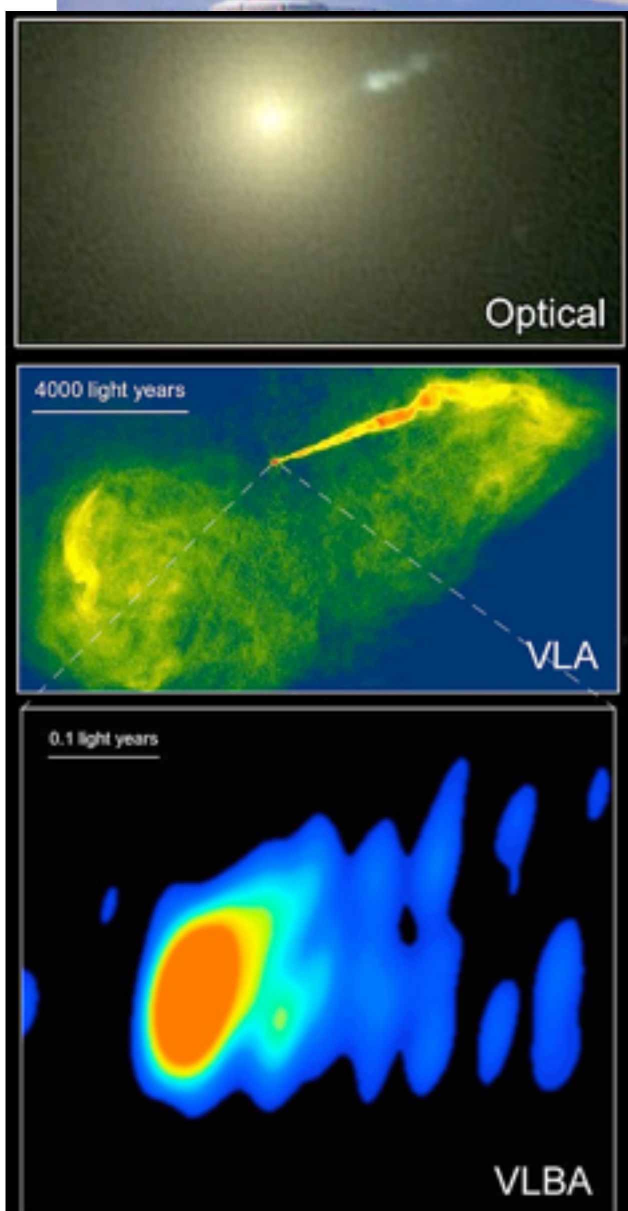

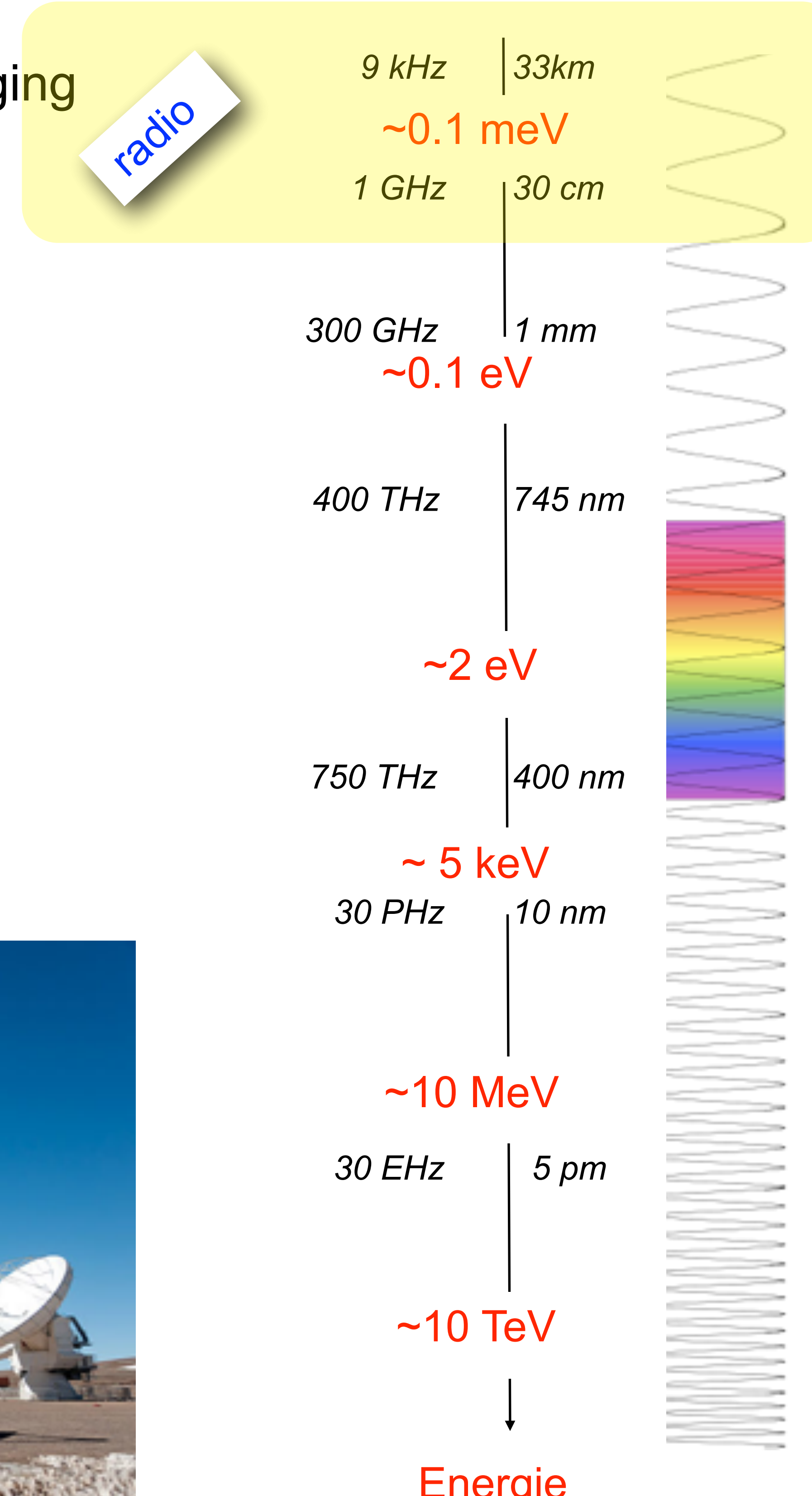

Photon imaging

LIght Detection And Ranging

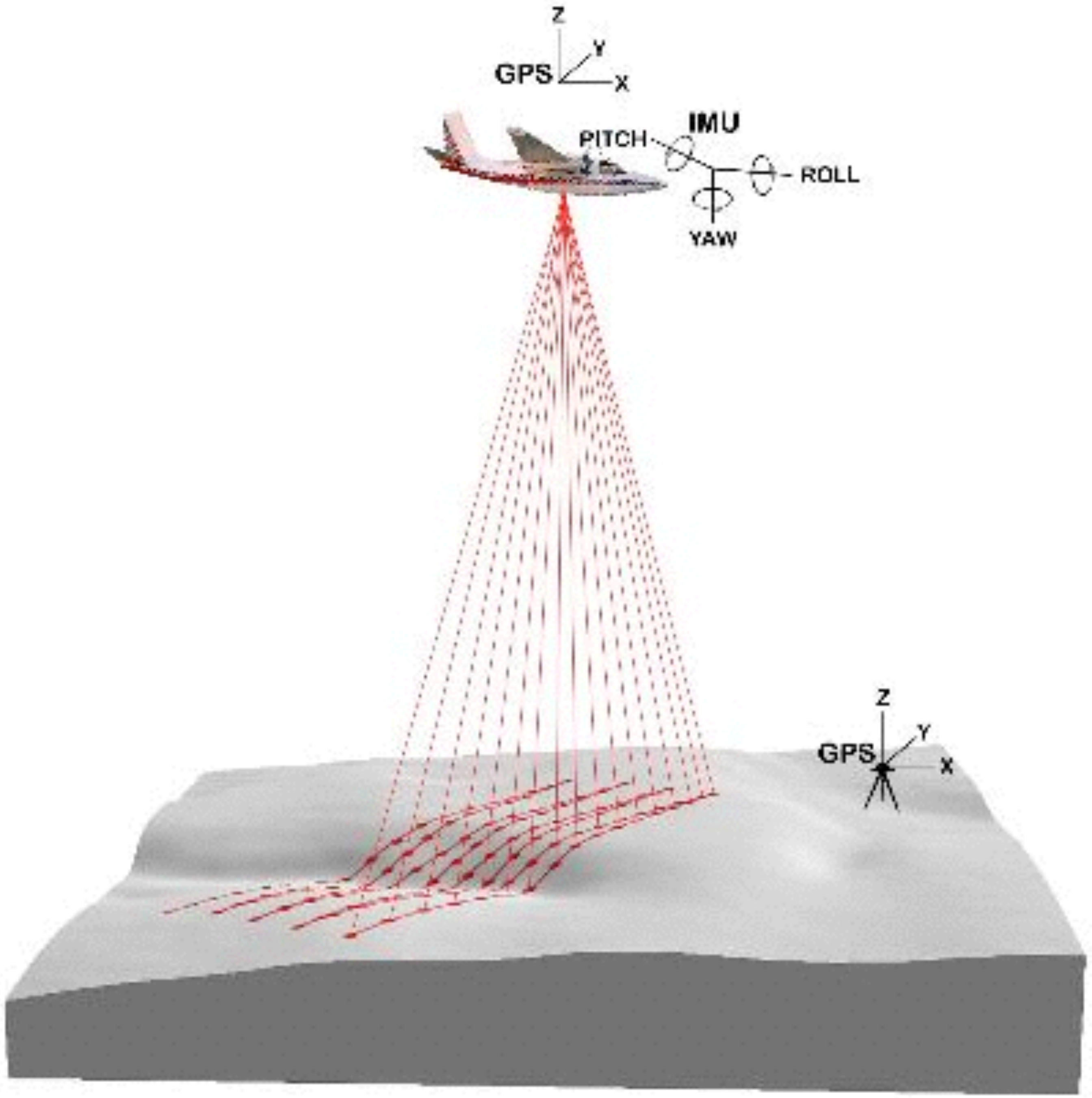

http://forsys.cfr.washington.edu/JFSP06/lidar_technology.htm


CUSTOMS

Muons: Id card

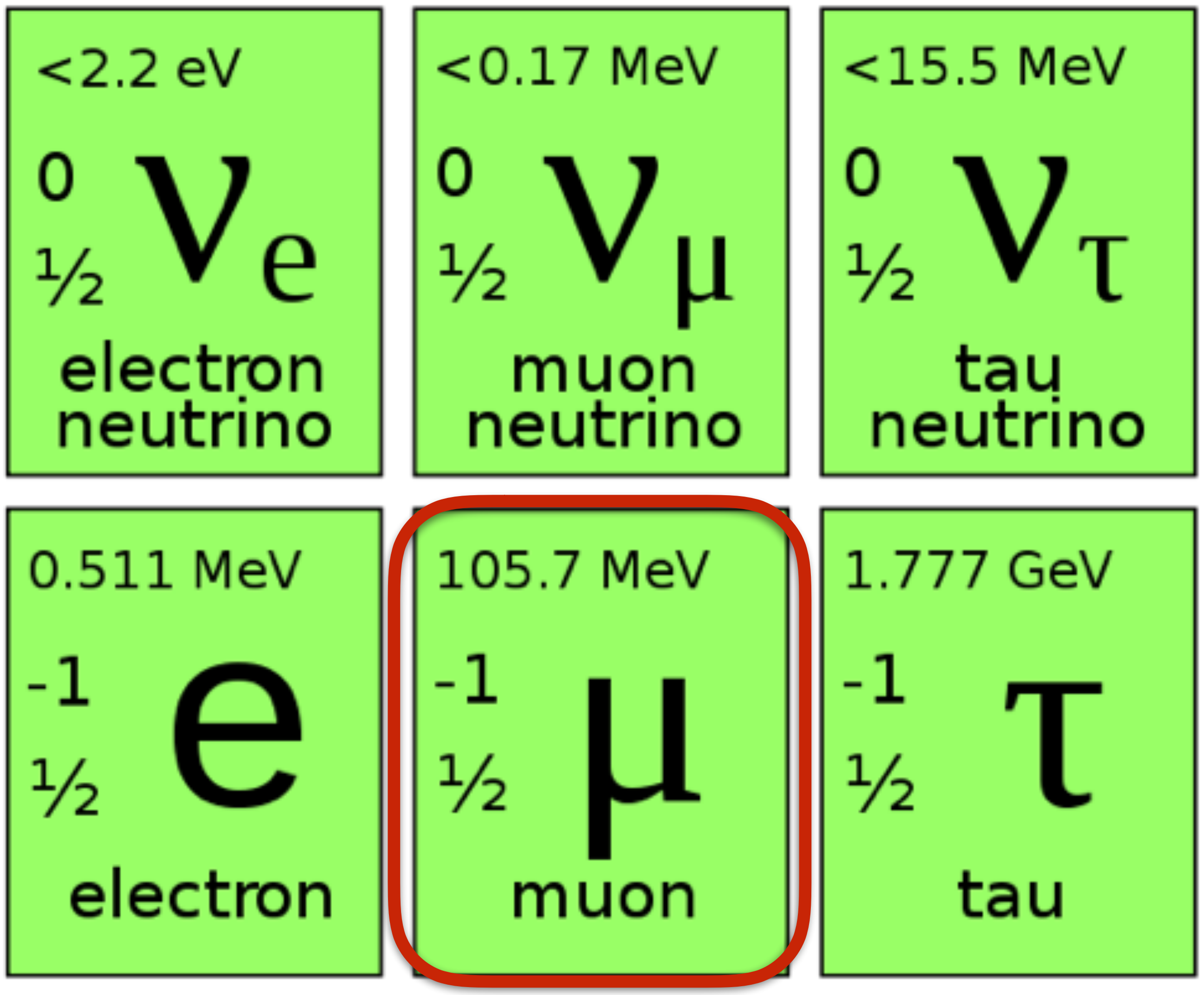

$\tau_\mu = 2.197\ \mu s$

$\mu^+ \rightarrow e^+ + \nu_e + \bar{\nu}_\mu$, $\mu^- \rightarrow e^- + \bar{\nu}_e + \nu_\mu$

Lifetime

- probability in $\exp(-t/\tau)$
- decay length: $l(p) = \frac{tp}{m}$

mass=105.7 MeV
$\tau 0 = 2.197\ \mu s$

$$\tau = \tau 0 / \sqrt{1 - v2 / c2}$$

E=750 MeV -> dilatation factor 10
E=10 GeV -> dilatation factor 100

… 6 km @ 1 GeV

@Particle Data Book
http://pdg.lbl.gov/

Muons for free in the atmospheric showers

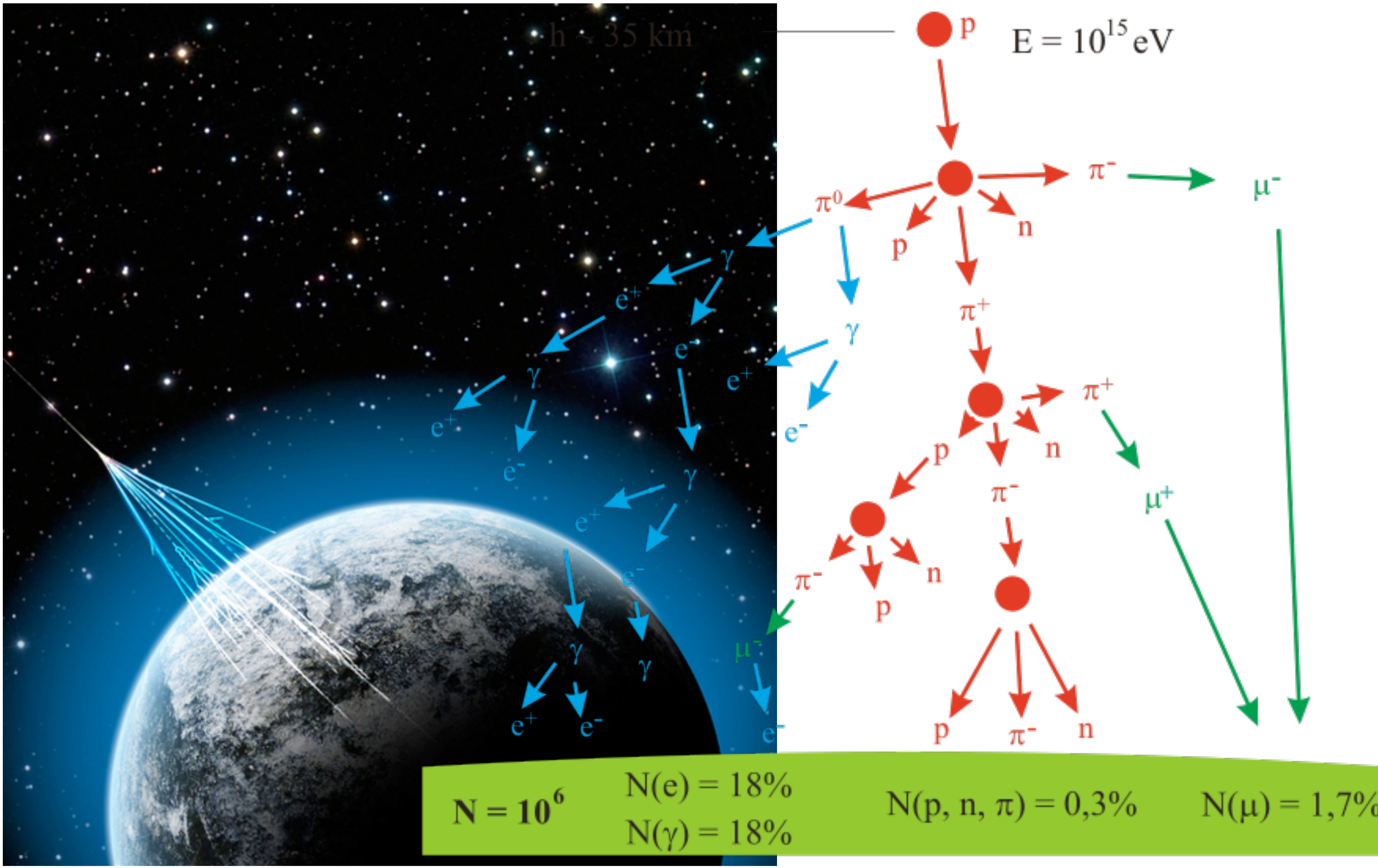

Atmospheric muons

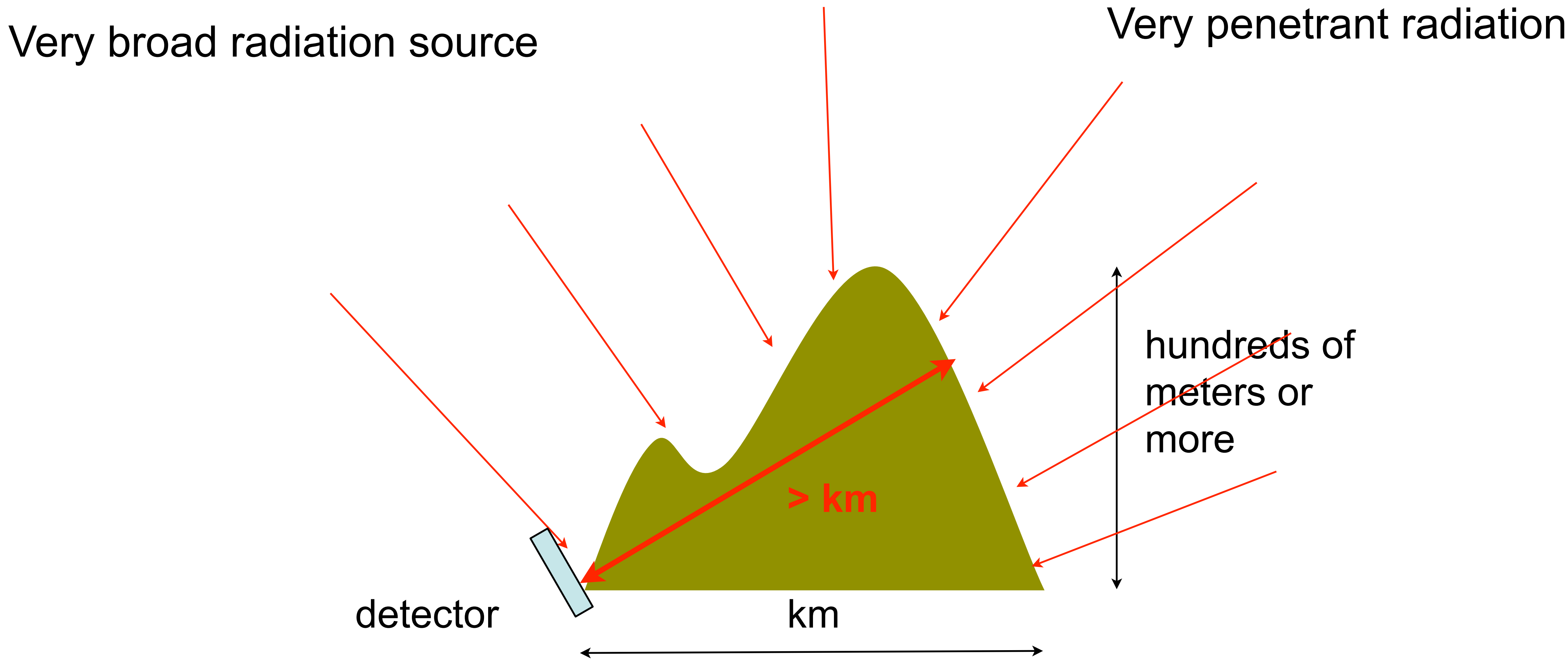

$$- \langle dE_\mu/dx \rangle = \alpha\,(E_\mu) + \beta\,(E_\mu)\,E_\mu$$

$$\langle R_\mu(E_\mu) \rangle = \int_0^{E_\mu} dE_\mu \,/\, \langle \Delta E/dx \rangle \sim \beta^{-1} \ln(1+\beta/\alpha\, E_\mu)$$

standard rock:
A=22, Z=11,
ρ=2.65 gcm^{-3}

E_μ	10 GeV	100 GeV	1 TeV	10 TeV
R_μ	19m	155m	0.9km	2.3km

Early muographic attempts: George, 1955

Cosmic Rays Measure Overburden of Tunnel

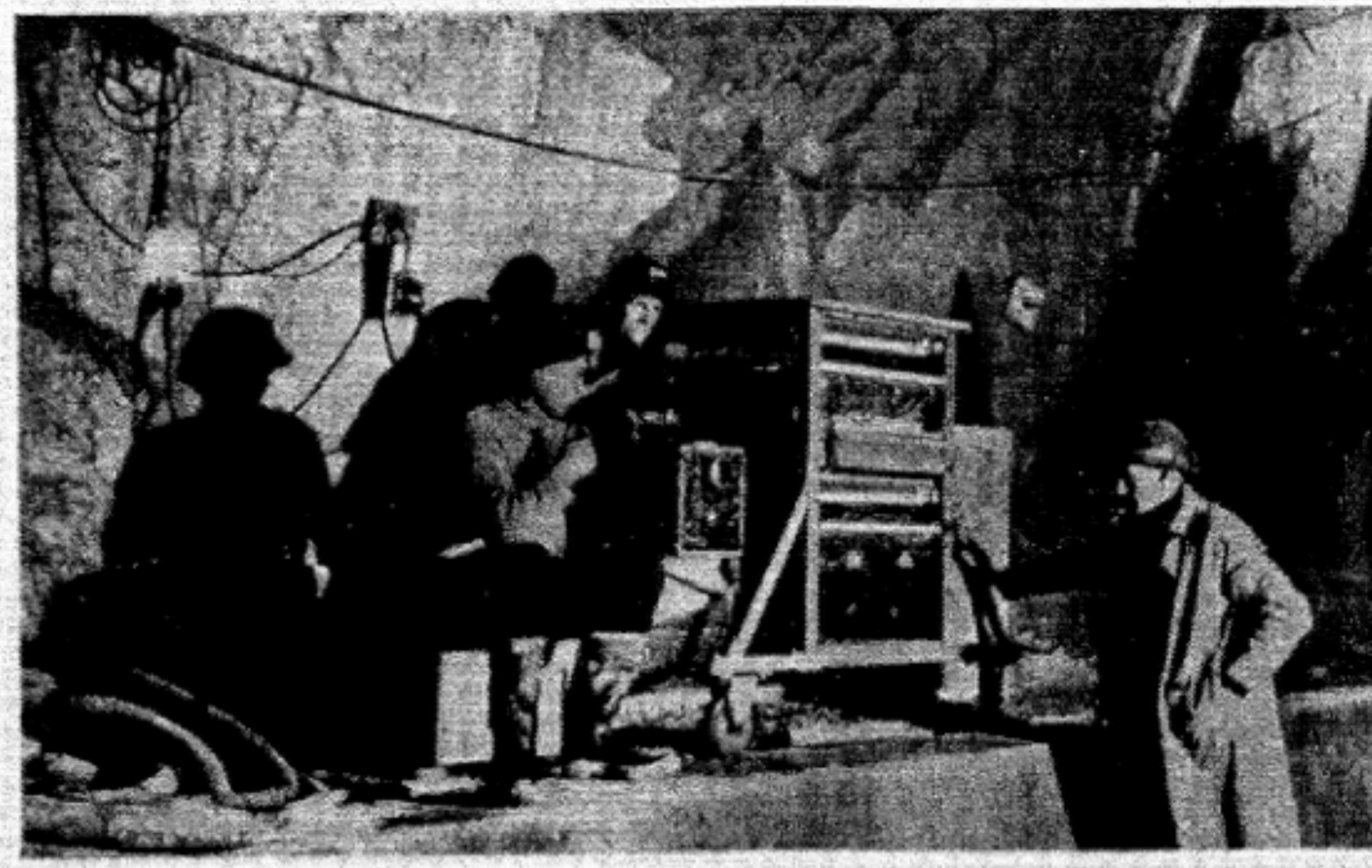

● Fig. 1—Geiger counter "telescope" in operation in the Guthega-Munyang tunnel. From left are Dr. George and his assistants, Mr. Lehane and Mr. O'Neill.

Geiger counter telescope used for mass determination at Guthega project of Snowy Scheme . . . Equipment described

By Dr. E. P. George*
University of Sydney, N.S.W.

Early muographic attempts: Alvarez 1970

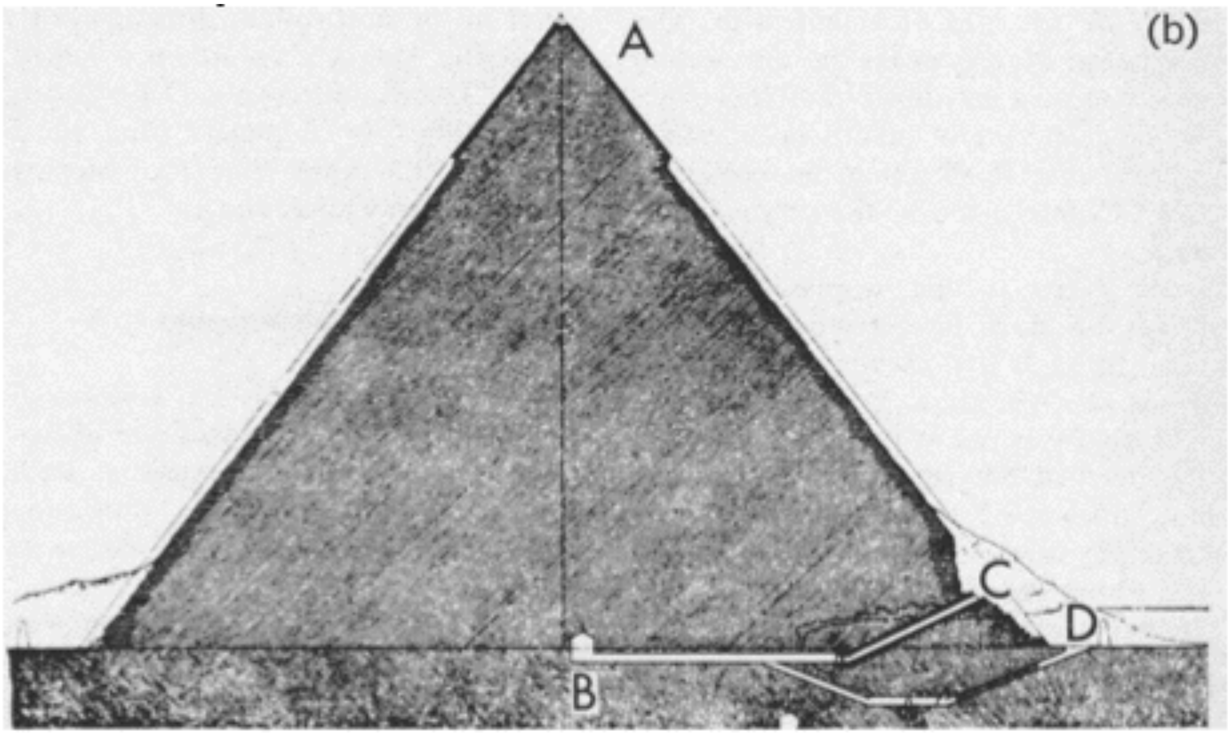

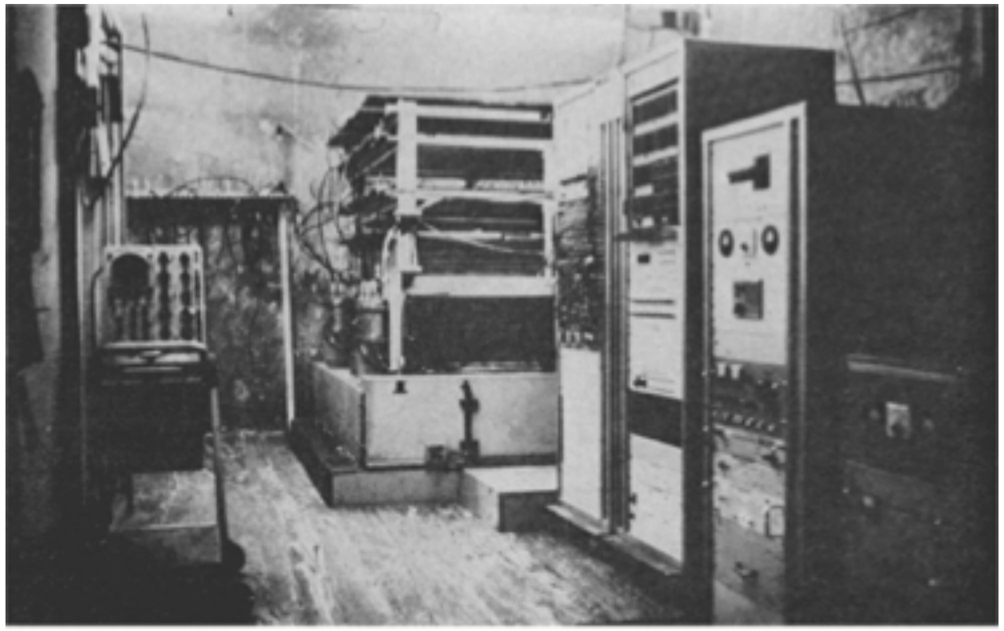

Fig. 6 (left). The equipment in place in the Belzoni Chamber under the pyramid.
Fig. 7 (right). The detection apparatus containing the spark chambers.

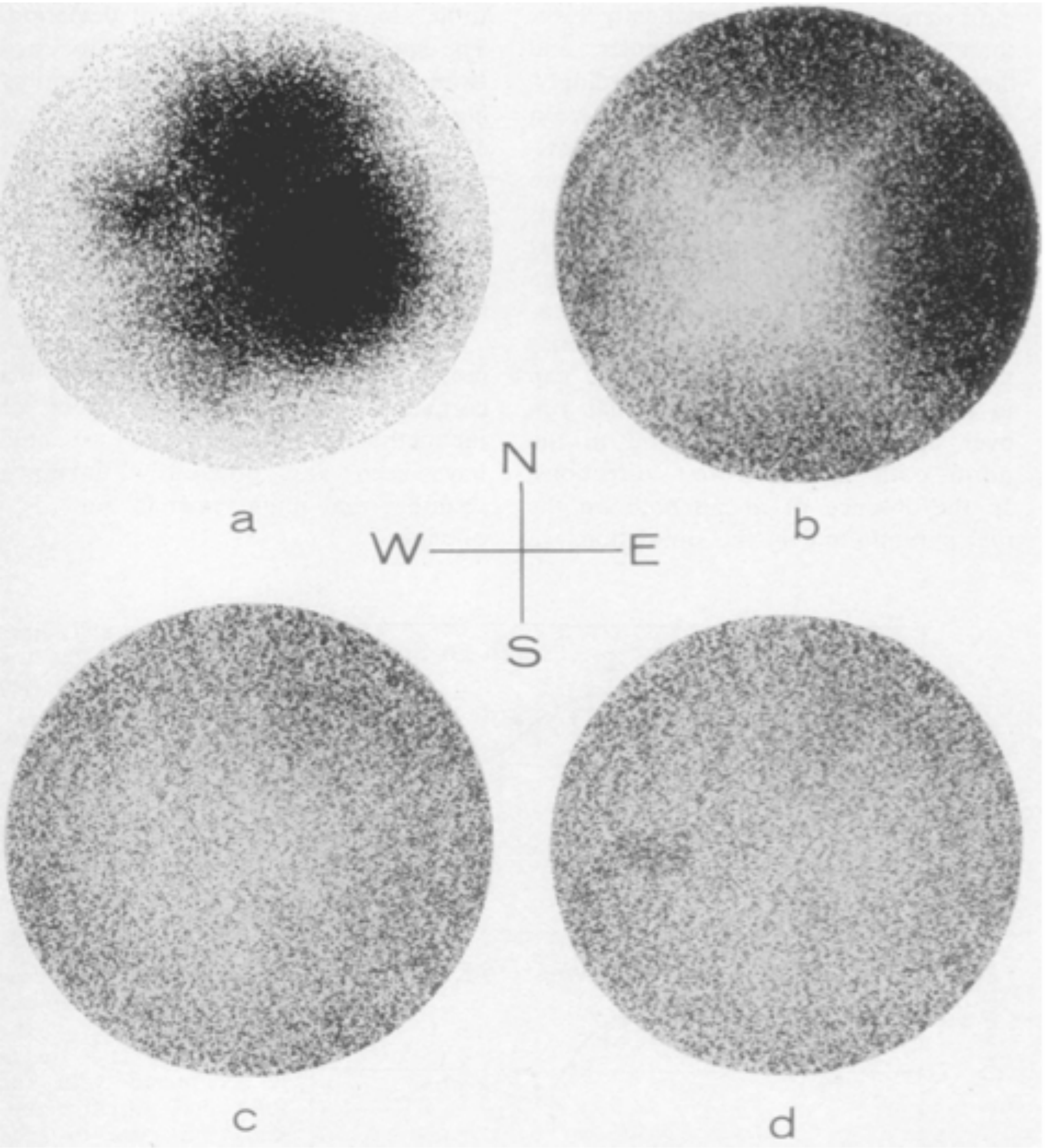

Fig. 13. Scatter plots showing the three stages in the combined analytic and visual analysis of the data and a plot with a simulated chamber. (a) Simulated "x-ray photograph" of uncorrected data. (b) Data corrected for the geometrical acceptance of the apparatus. (c) Data corrected for pyramid structure as well as geometrical acceptance. (d) Same as (c) but with simulated chamber, as in Fig. 12.

Muon energy loss

http://pdg.lbl.gov/2015/reviews/rpp2015-rev-passage-particles-matter.pdf

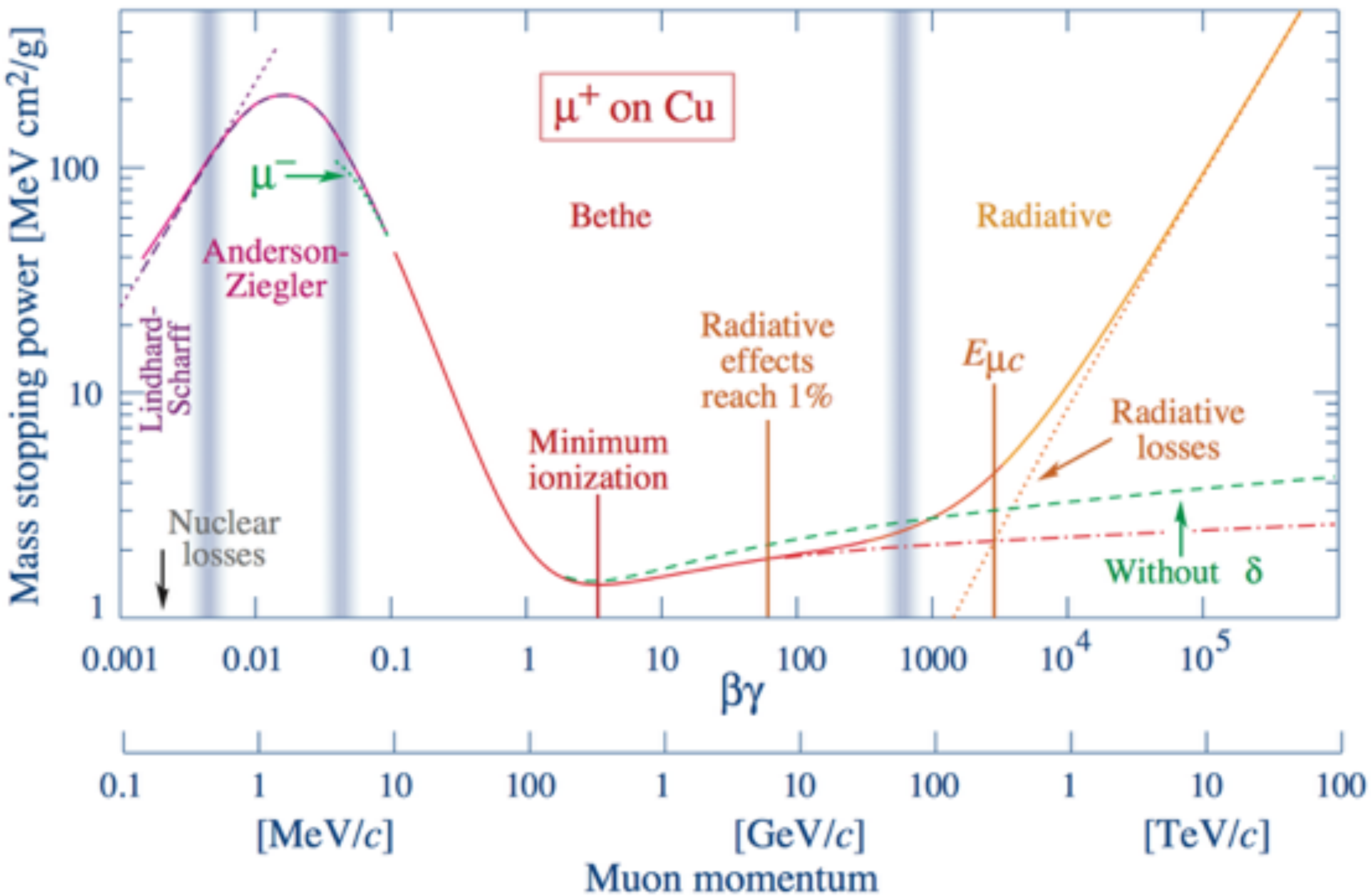

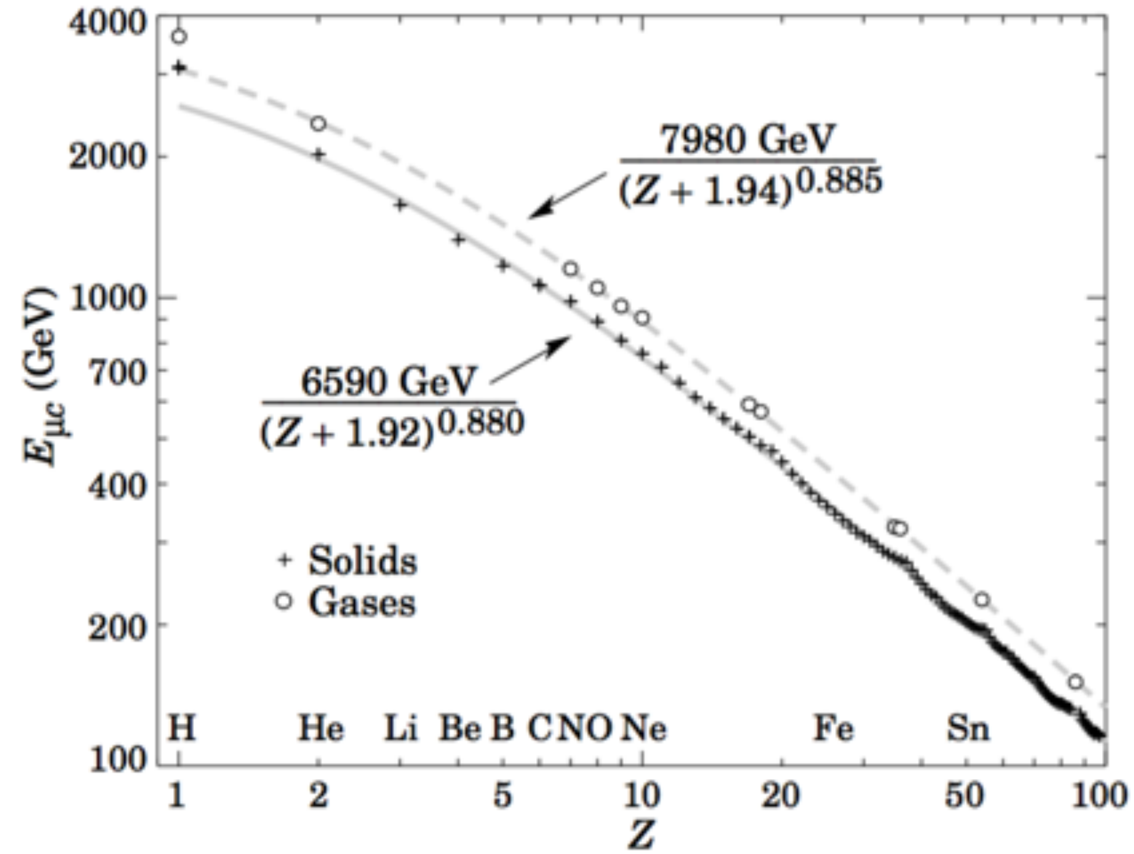

$$\frac{dE}{dx} = -4\pi r_e^2 m_e c^2 z^2 \frac{N_A Z}{A} \frac{1}{\beta^2}\left[\ln\frac{2m_e c^2\beta^2\gamma^2}{I\sqrt{1+\epsilon}} - \beta^2 - \frac{\delta}{2}\right]$$

Muon deflection

pdg.lbl.gov/2015/reviews/rpp2015-rev-passage-particles-matter.pdf

$$\theta_0 = \frac{13.6\ \mathrm{MeV}}{\beta c p} Z \sqrt{x/X_0}\Big[1 + 0.038 \ln(x/X_0)\Big]$$

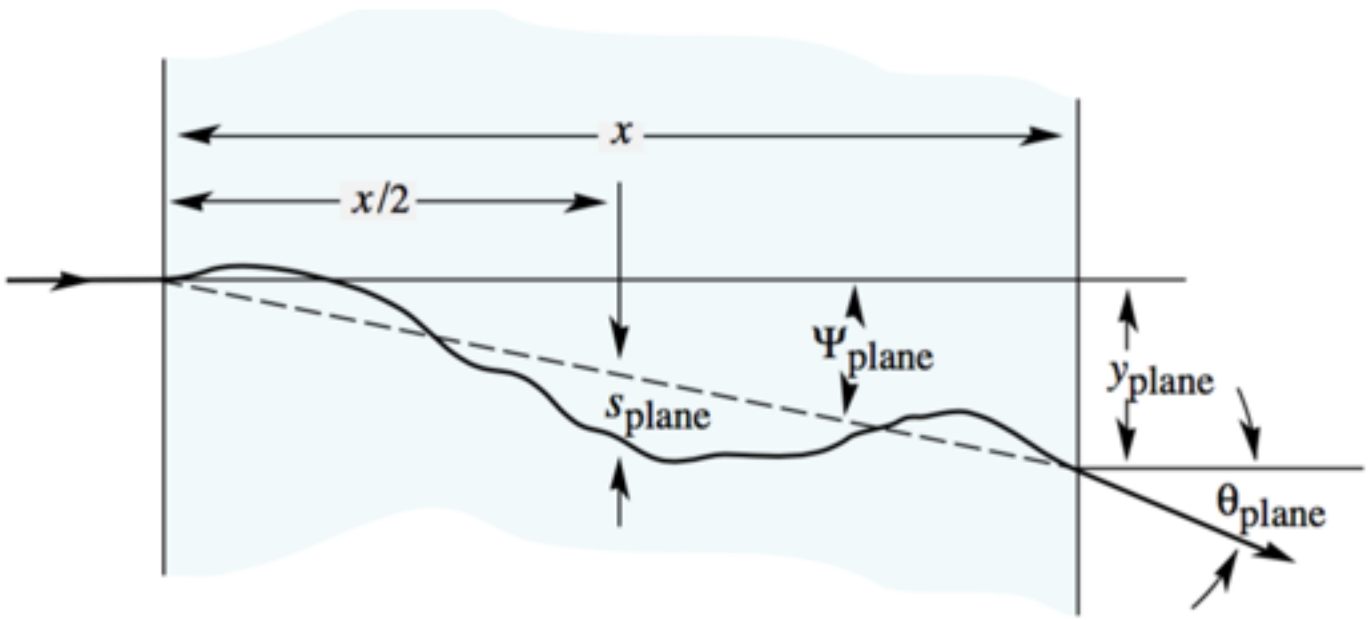

$$\frac{1}{X_0} = 4\alpha r_e^2 \frac{N_A}{A}\left\{Z^2\big[L_{\mathrm{rad}} - f(Z)\big] + Z\, L'_{\mathrm{rad}}\right\} .$$

Element	Z	L_{rad}	L'_{rad}
H	1	5.31	6.144
He	2	4.79	5.621
Li	3	4.74	5.805
Be	4	4.71	5.924
Others	> 4	$\ln(184.15\, Z^{-1/3})$	$\ln(1194\, Z^{-2/3})$

Two exploitable interactions

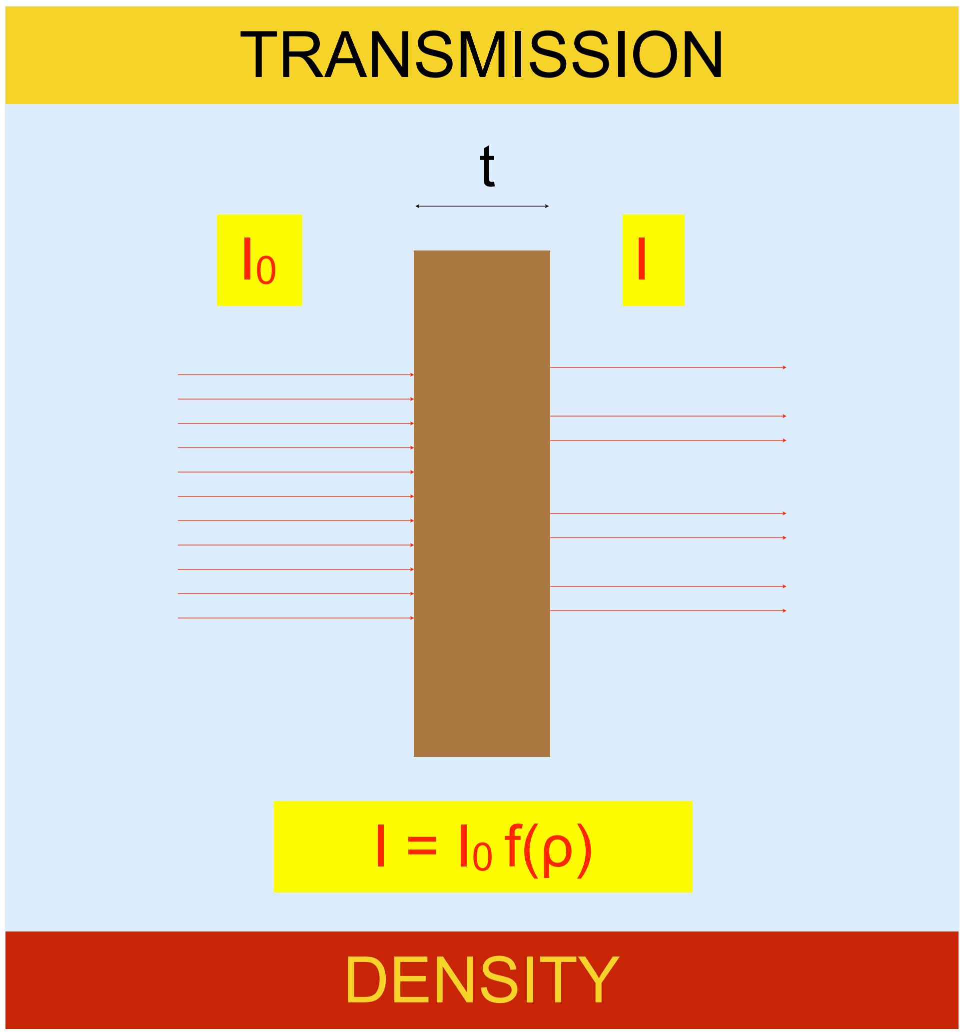

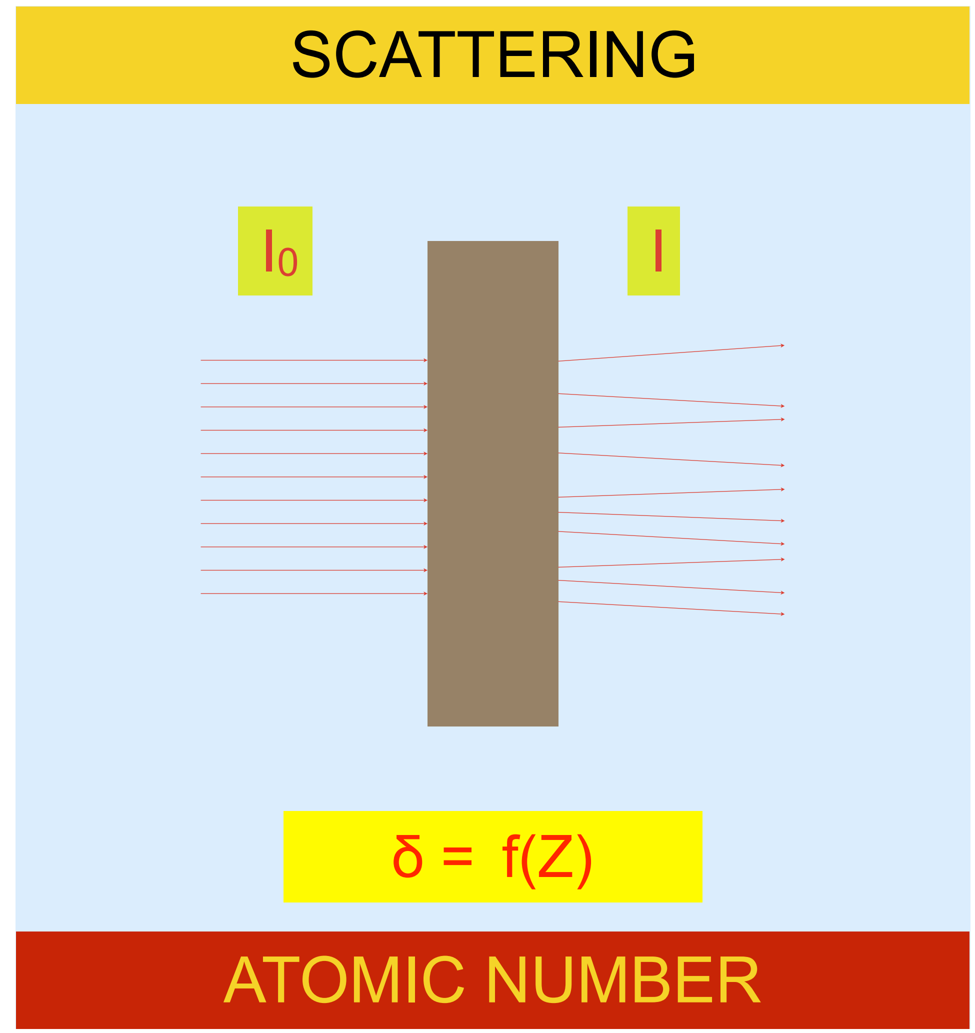

- 2D image
- applicable to very large targets
- relies on incident flux knowledge

- 3D image
- necessary to measure each individual track before and after the target
- small to medium targets
- high position resolution, large area detectors

Diffusion muography: very active research field

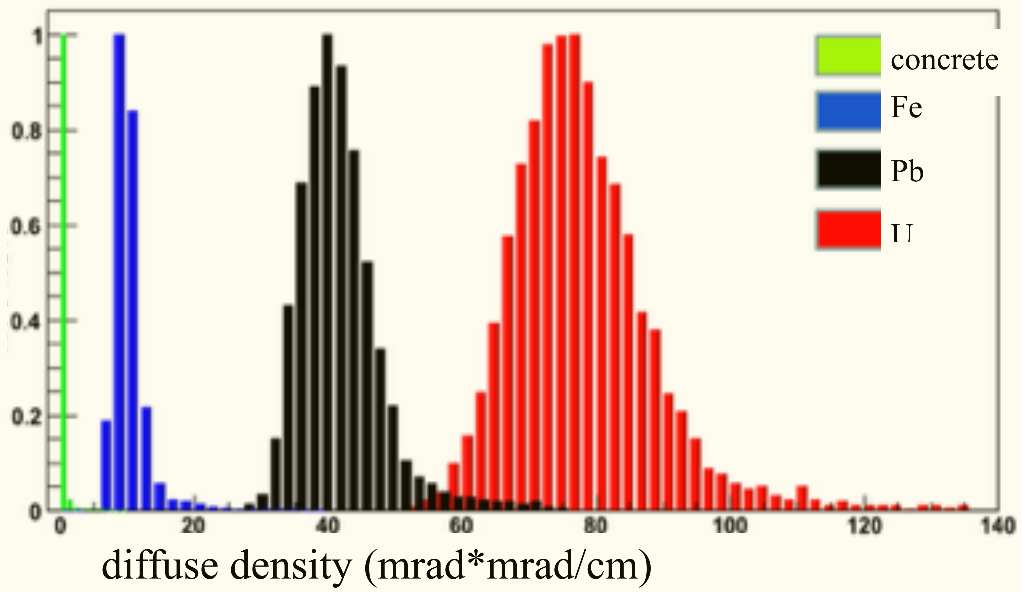

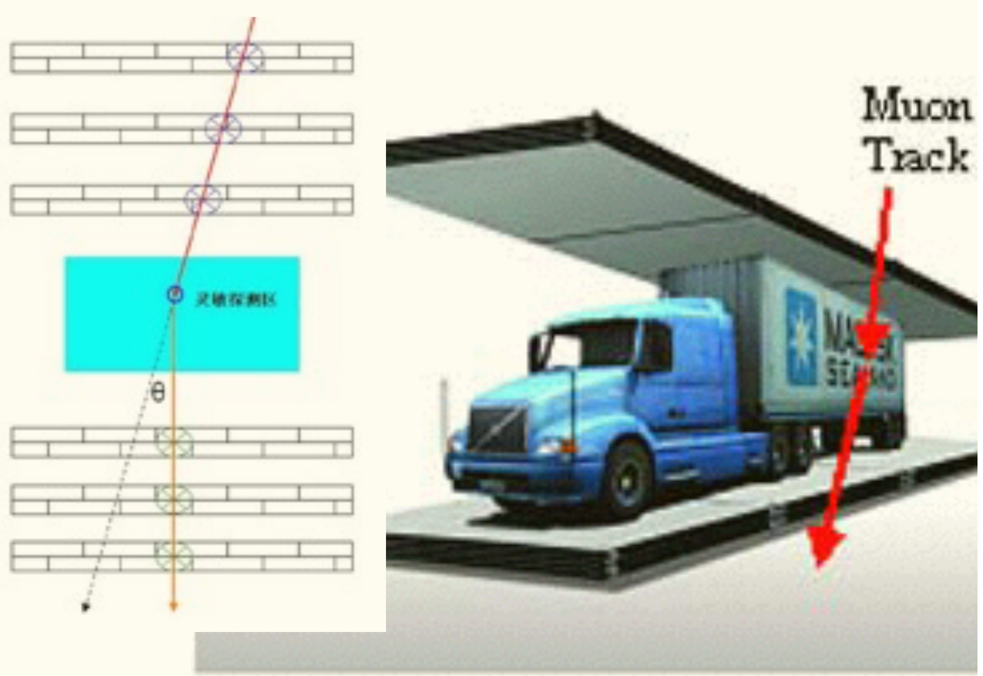

Energy & Environment | New Nuclear | Regulation & Safety | Nuclear Policies | Corporate | Uranium &

Muon data confirms fuel melt at Fukushima Daiichi 1

23 March 2015

Initial results from using a muon detection system at the damaged Fukushima Daiichi unit 1 in Japan appear to confirm that most of the fuel has melted and dropped from its original position within the core, Tokyo Electric Power Company (Tepco) announced.

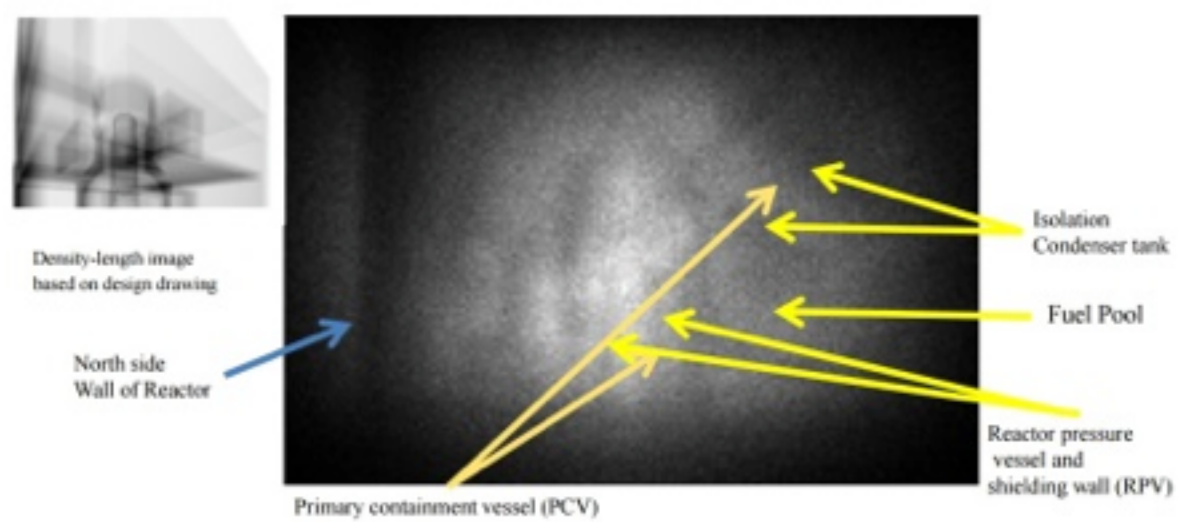

Results obtained from the muon detector on the northwest side of the reactor building (Image: Tepco)

The company completed installation of the muon detection system on 12 February. Two detectors were installed: one on the northwest side of the reactor building and the other on the north side. Since then, data collection continued until 10 March (a period of 26 days). The initial results have now been analysed.

The detector system was developed by Japan's High Energy Accelerator Research Organization (KEK). The system uses the so-called permeation method to measure the muon data.

Related Stories

- Looking inside Fukushima Daiichi unit 1
- Cosmic rays to pinpoint Fukushima cores
- Fukushima fuel melt confirmed

WNA Links

- Fukushima Daiichi 1
- The Situation at Fukushima

Related Links

- Tokyo Electric Power Co. (Tepco)

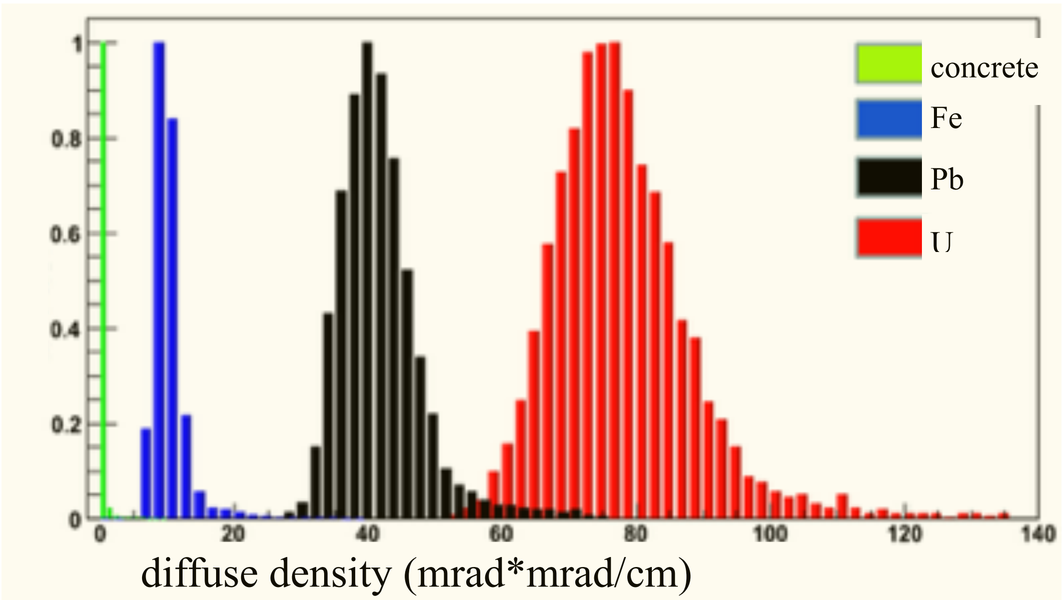

concrete
Fe
Pb
U
0
0.2
0.4
0.6
0.8
1
0
20
40
60
80
100
120
140
diffuse density (mrad*mrad/cm)

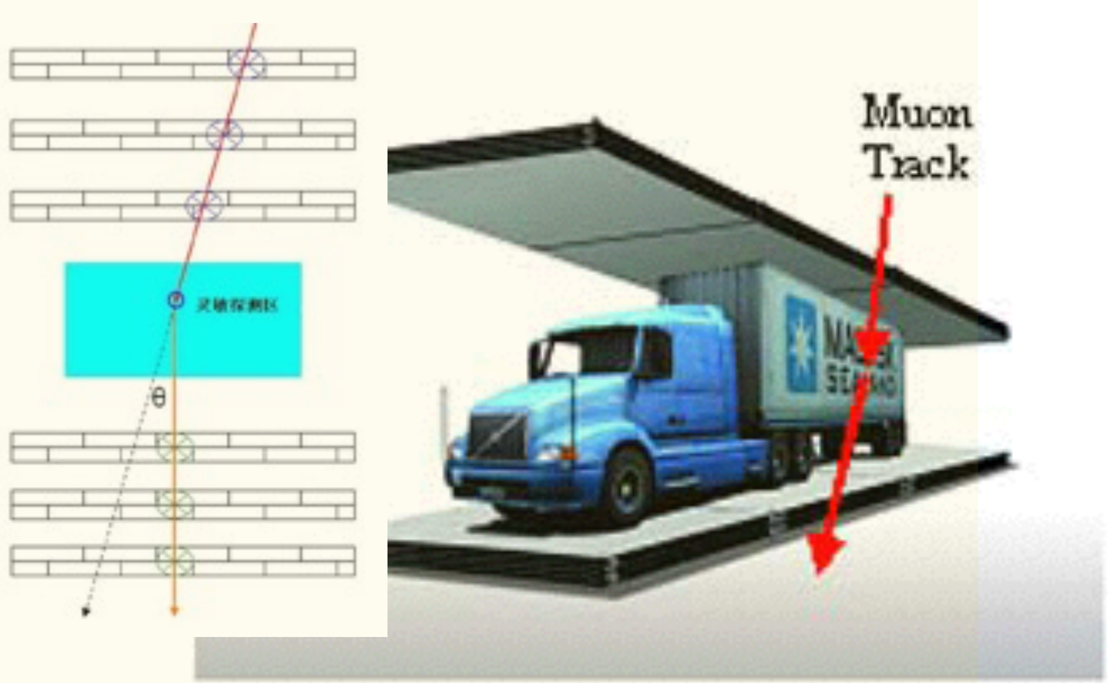

θ
Muon
Track

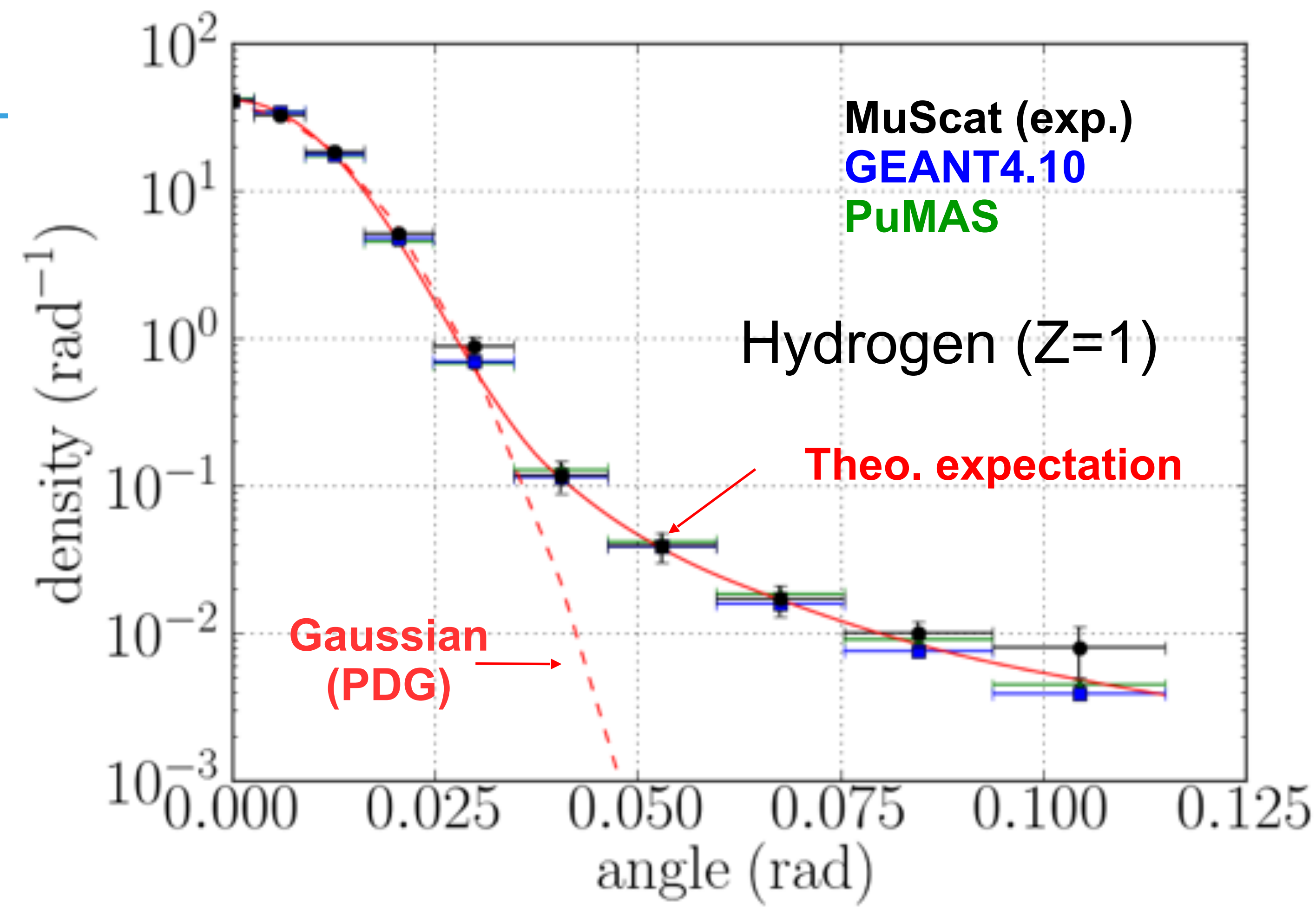

MuScat (exp.)
GEANT4.10
PuMAS
Hydrogen (Z=1)
Theo. expectation
Gaussian
(PDG)
density (rad^{-1})
10^2
10^1
10^0
10^{-1}
10^{-2}
10^{-3}
0.000
0.025
0.050
0.075
0.100
0.125
angle (rad)

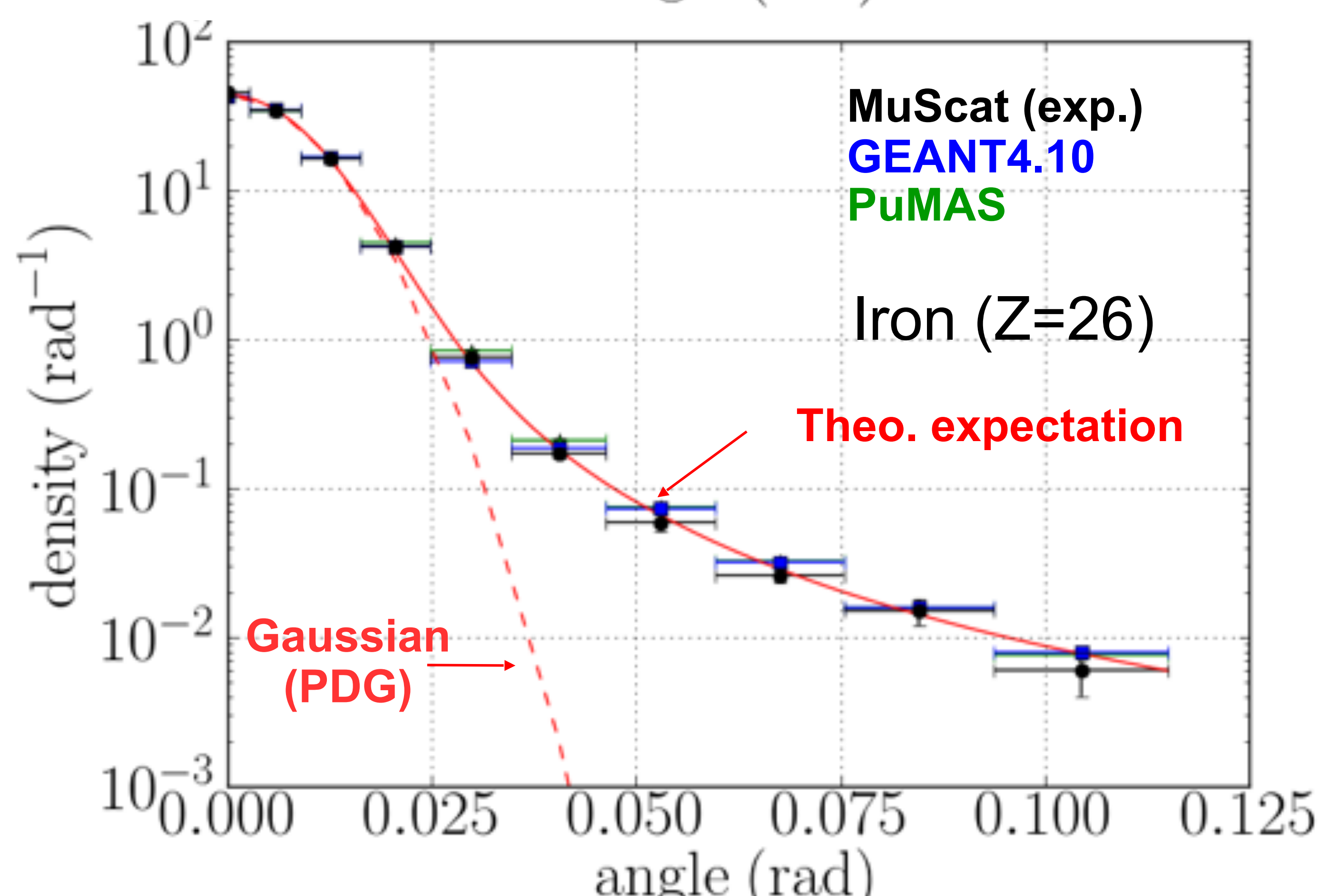

MuScat (exp.)
GEANT4.10
PuMAS
Iron (Z=26)
Theo. expectation
Gaussian
(PDG)
density (rad^{-1})
10^2
10^1
10^0
10^{-1}
10^{-2}
10^{-3}
0.000
0.025
0.050
0.075
0.100
0.125
angle (rad)

Transmission muography in a nutshell ...

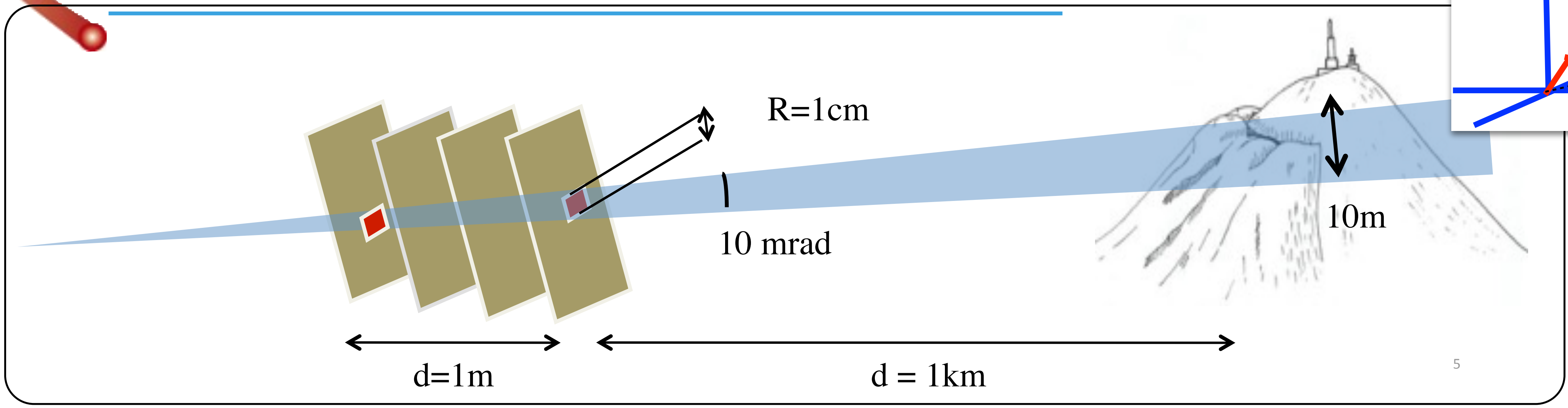

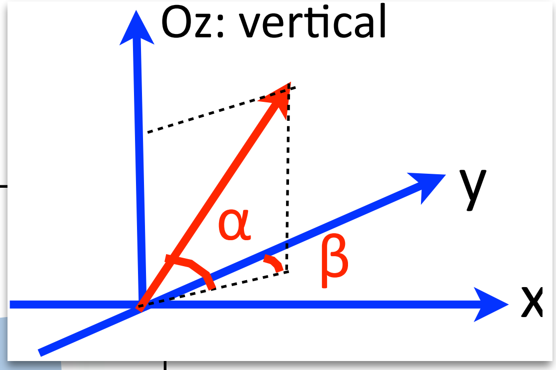

$$\mathcal{T}_{\rho}(\alpha, r(\alpha,\beta)) = \frac{\Phi(\alpha, r(\alpha,\beta))}{\Phi_0(\alpha)}$$

$$\boxed{\int \rho(\alpha,\beta)dr = \mathcal{F}(\mathcal{T}(\alpha,\beta))}$$

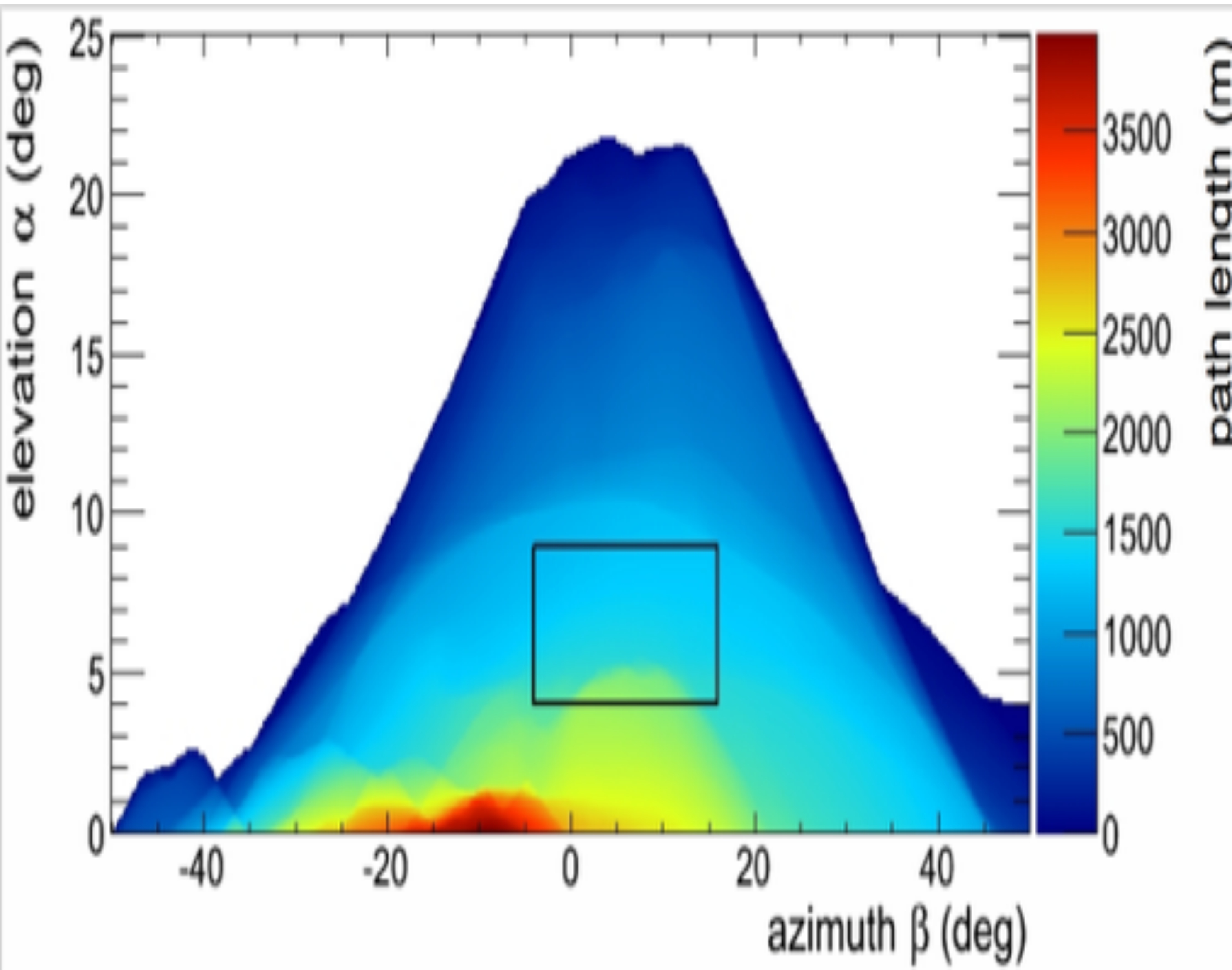

WHY

Physics case: volcano structure imaging

Various hazards with different physical causes and magnitudes

- phreato-magmatic explosion
- phreatic explosion (release of thermal energy contained in the hydrothermal reservoirs)
- landslide and flank collapse (may be triggered by internal overpressure, earthquake)

Hazard level depends on present-day state of the volcano

- Degree of alteration (mechanical integrity)
- Volume of reservoirs (stored energy)
- Internal changes (liquid/vapor transition)
- Channels and conduits

Structure imaging plays a leading role in hazard prediction

Physics case: why structure imaging

Structure understanding - key to comprehension and prediction


EUROPE'S TICKING TIME BOMB
@ NATURE, VOL 143, 12 May 2011

Physics case: monitoring eruptions?

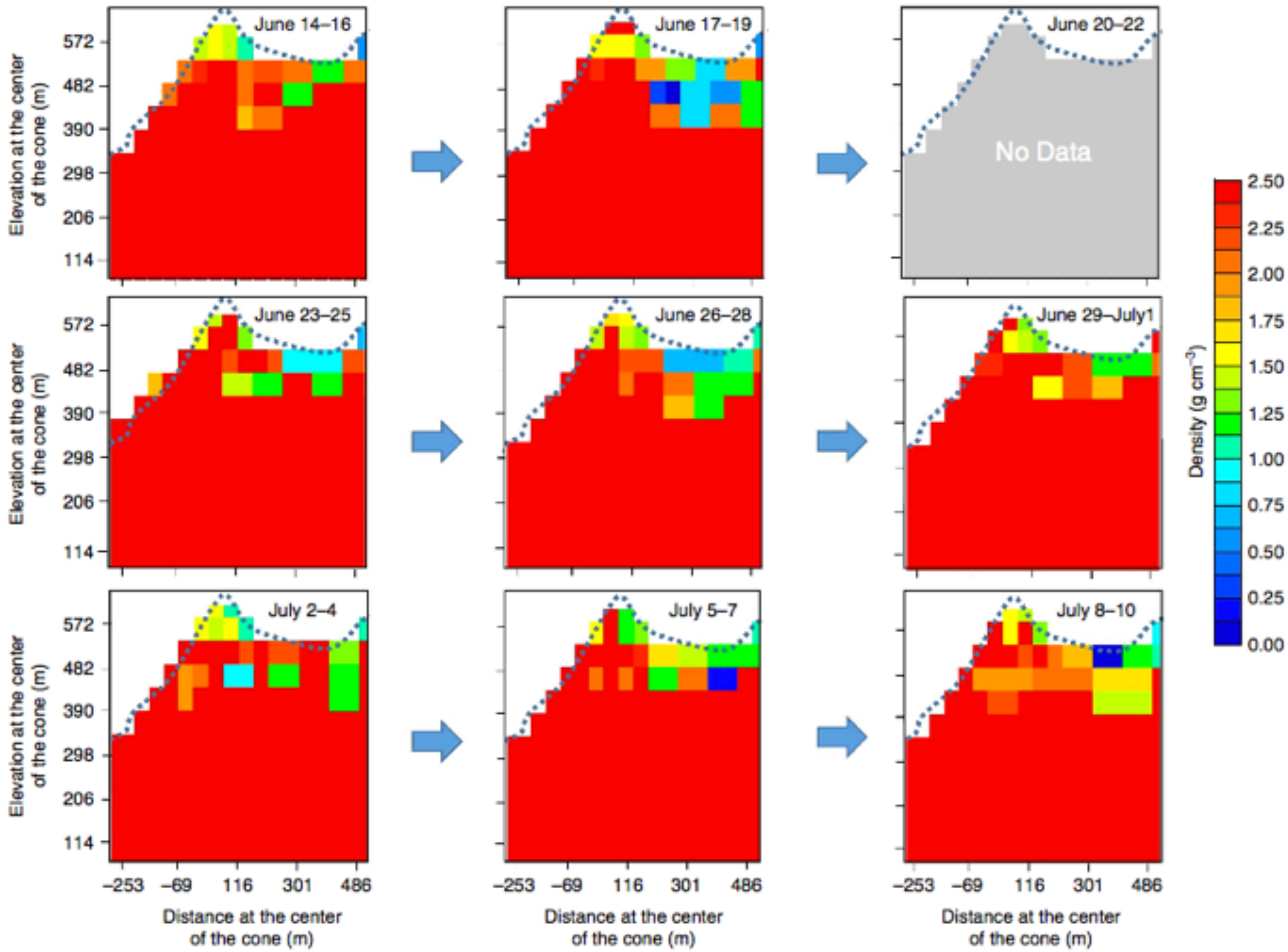

Figure 5 | Time sequential muographic animation. The plots show the angular distribution of 1σ (68% CL) upper limit of the average density along the muon path. The frame rate is 10 FPM. The data were not taken during 20-22 June due to a blackout. Horizontally adjacent two bins were packed in order to achieve higher and more accurate statistics. The elevation and horizontal distances at the centre of the cone are shown.

NATURE COMMUNICATIONS | 5:3381 | DOI: 10.1038/ncomms4381 | www.nature.com/naturecommunications

7

Physics case: volcano structure imaging

Structure imaging plays a leading role in hazard prediction

- Electrical conductivity : resistivity
- Seismic waves velocity + coda waves : elasticity
- Gravimetry and muography : density

Geophys. methods for volcano imaging: electrical resistivity

Vulcano, Stromboli (Iles Eoliennes; Italie)

Finizola et al., GRL (2006, 2009); Revil et al., JGR (2008)

Electrical resistivity of Puy de Dôme

Portal et al, EGU 2016-8549,

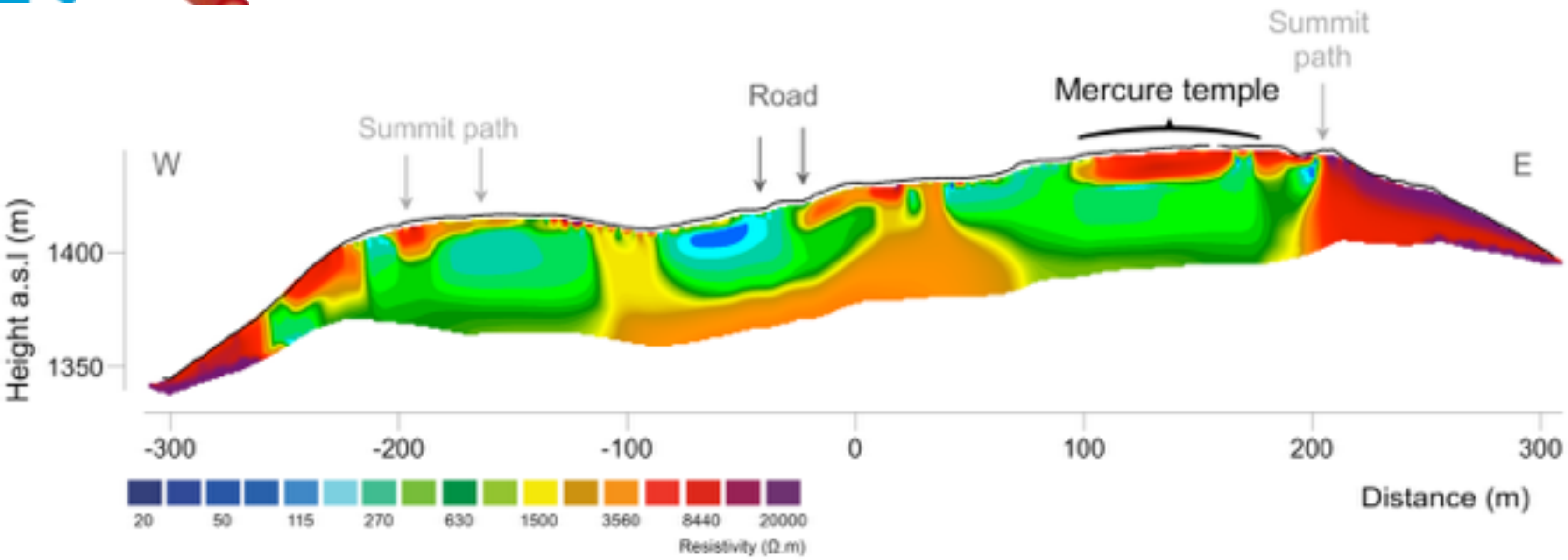

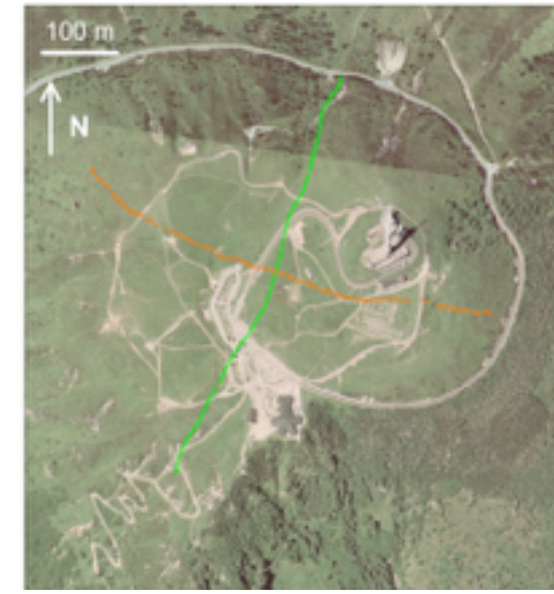

Erreur rms 7.3%

Anthropic structures

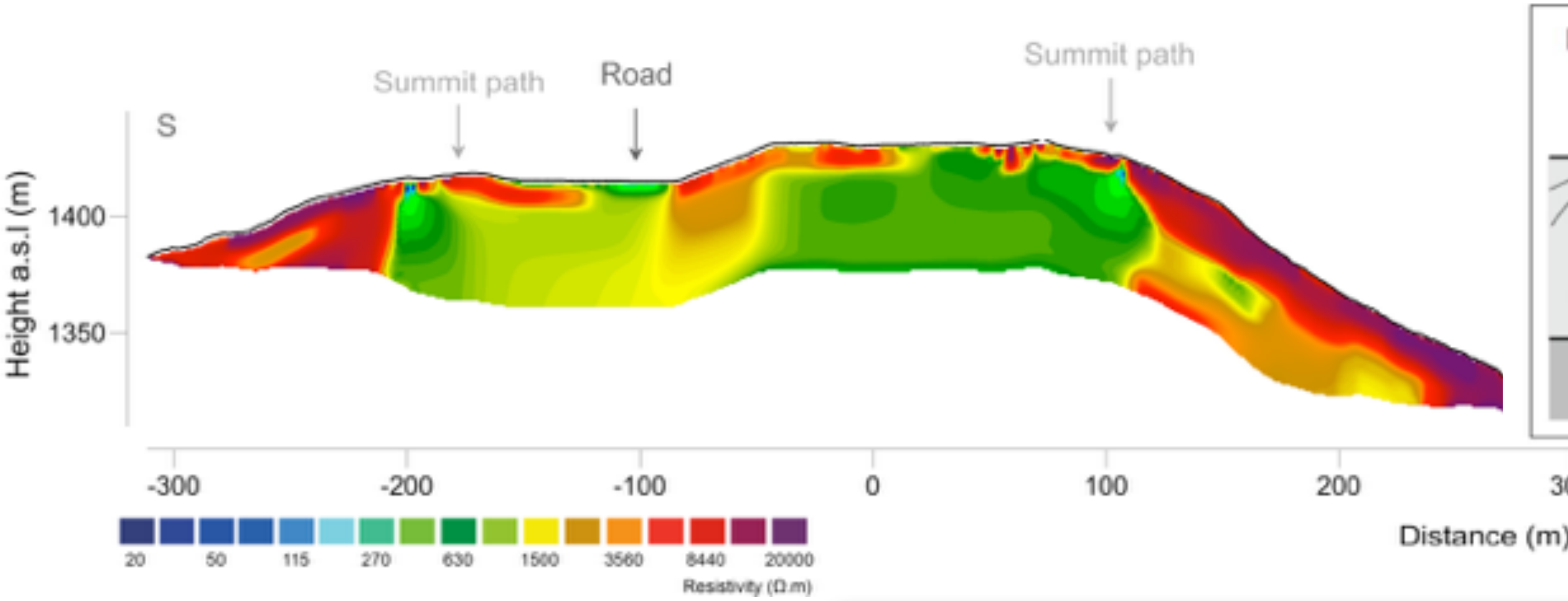

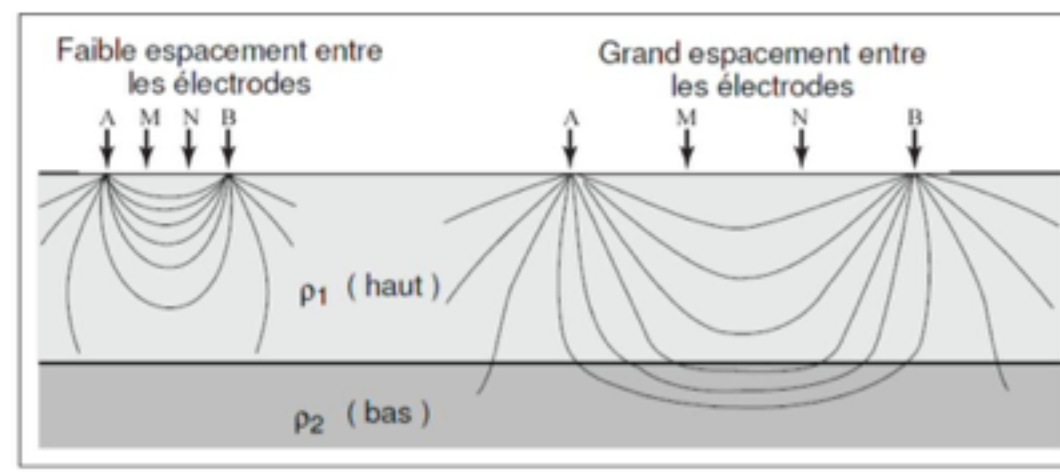

Erreur rms 6.8%

Computed with Res2DInv *(Loke, 2011)*

Seismic and electrical tomography rely on curved paths

⇓

non-linear inverse problem

Geophys. methods for volcano imaging: micro-gravimetry

- Relative gravimeter (February-March, 2012, May, 2012 and March-June, 2013)
- 610 gravity stations, around 2500 gravity measurements
- High resolution differential GPS positioning at the gravimeter tripod center

  ↳ average accuracy: **1.6 cm** in planimetry and **2.3 cm** in altimetry

GPS and Scintrex CG5 gravimeter

Portal et al, JVGR, 2016

Gravity stations location for the total survey

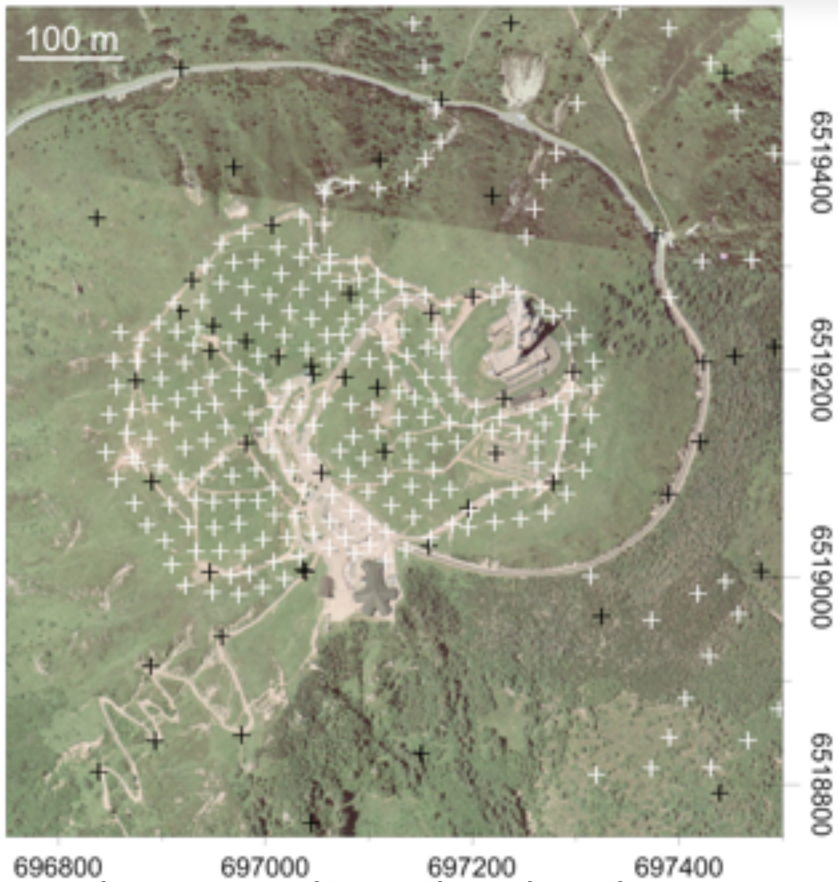

Summit area gravity stations location

Inverse problem in gravimetry

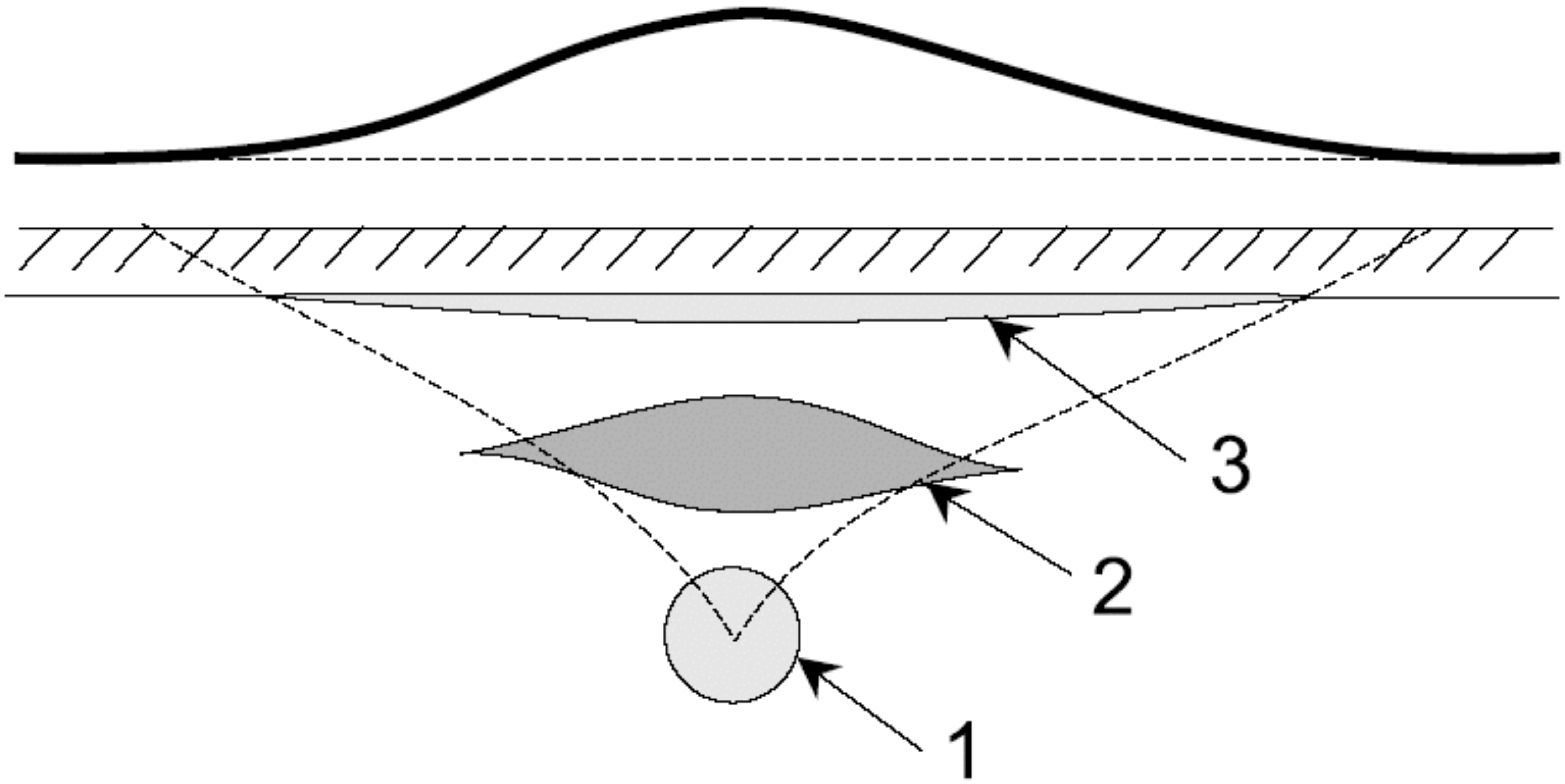

Micro-gravimetry of Puy de Dôme

The Chaîne des Puys volcanic field

- The latest active zone of the French "Massif Central" volcanism
- Important rifting episode -> hemi-graben formation (*Michon and Merle, 2001; Boivin and al., 2004*)
- Volcanoes emplaced on a Hercynian granitic basement along a N-10° direction

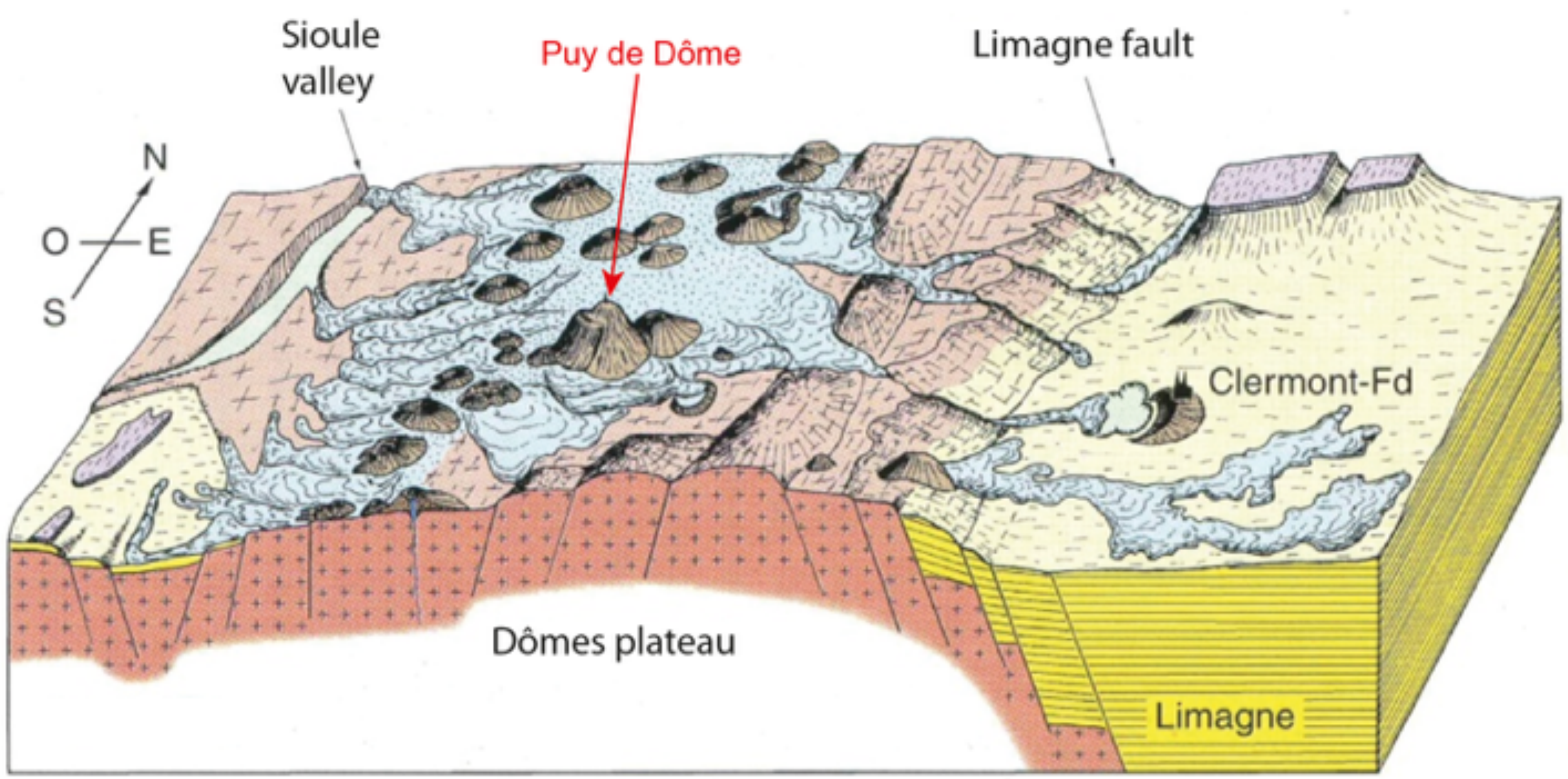

Figure Boivin and al., 2004

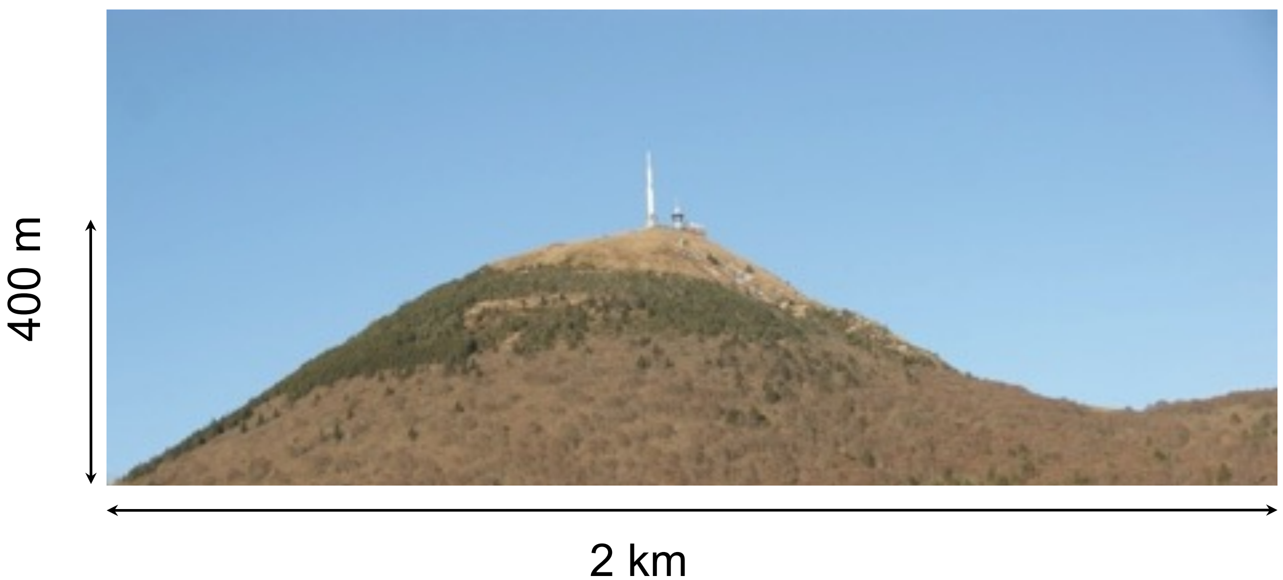

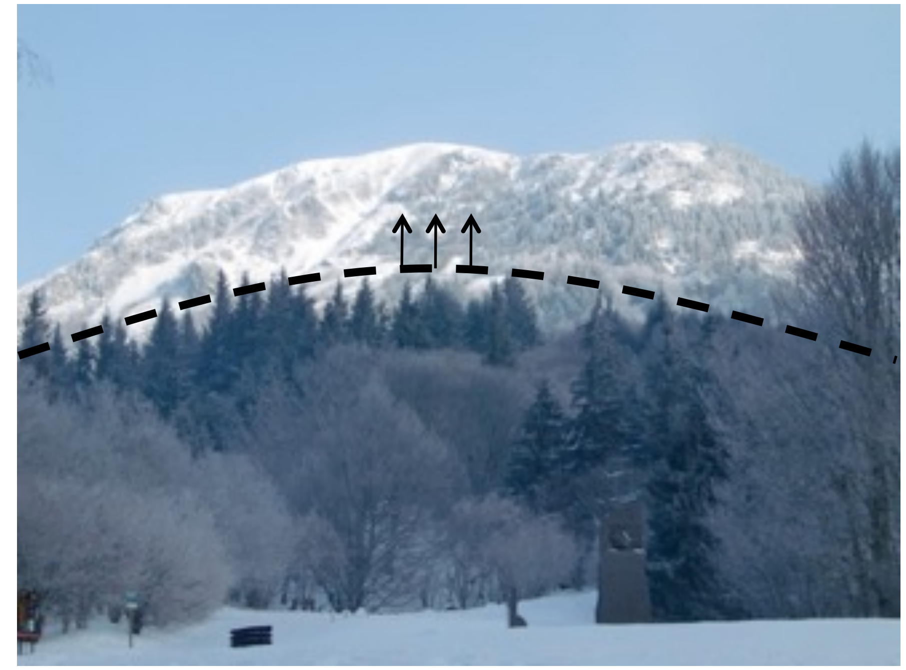

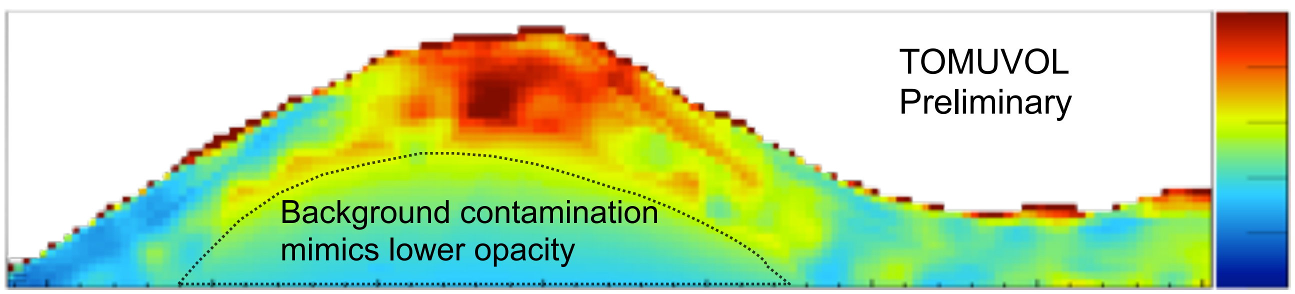

Linear opacity to atmospheric muons
65.8 days of data taking, 0.16 m^2 x 0.5 m

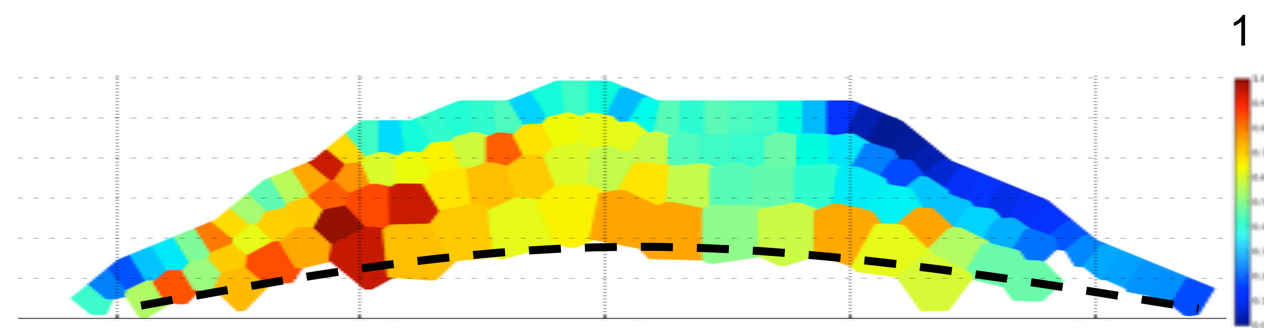

Density contrast
14 days of data taking, 0.66 m^2 x 1 m

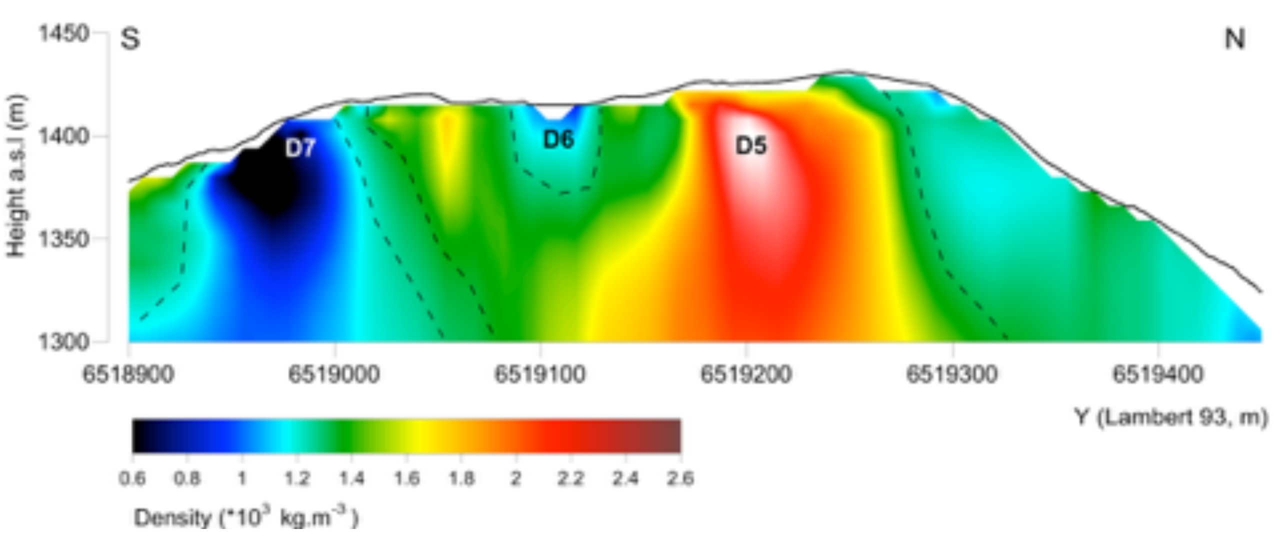

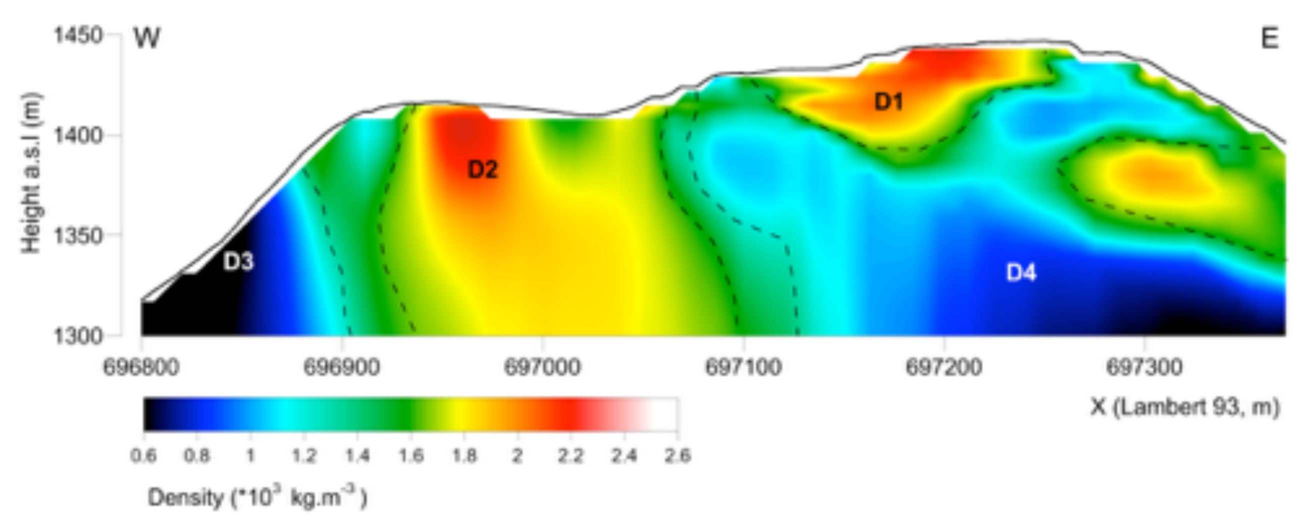

Inverse problem : muon flux

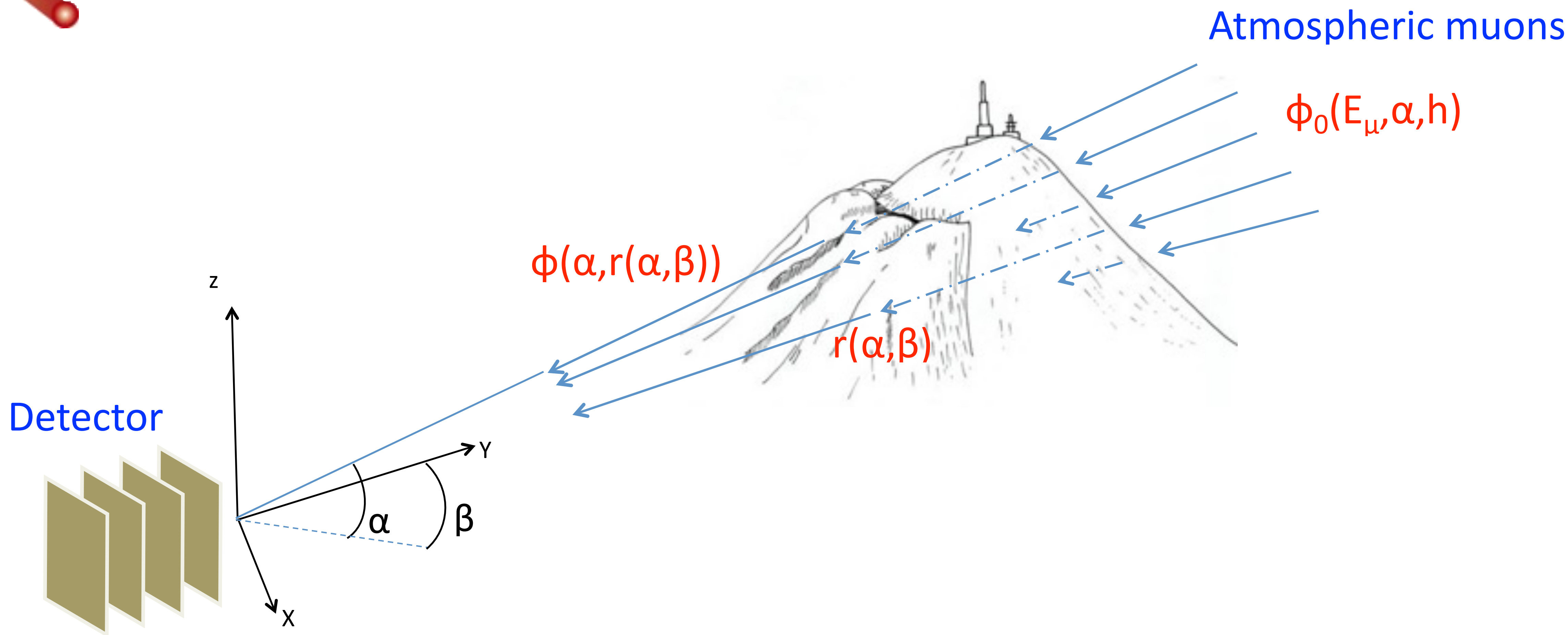

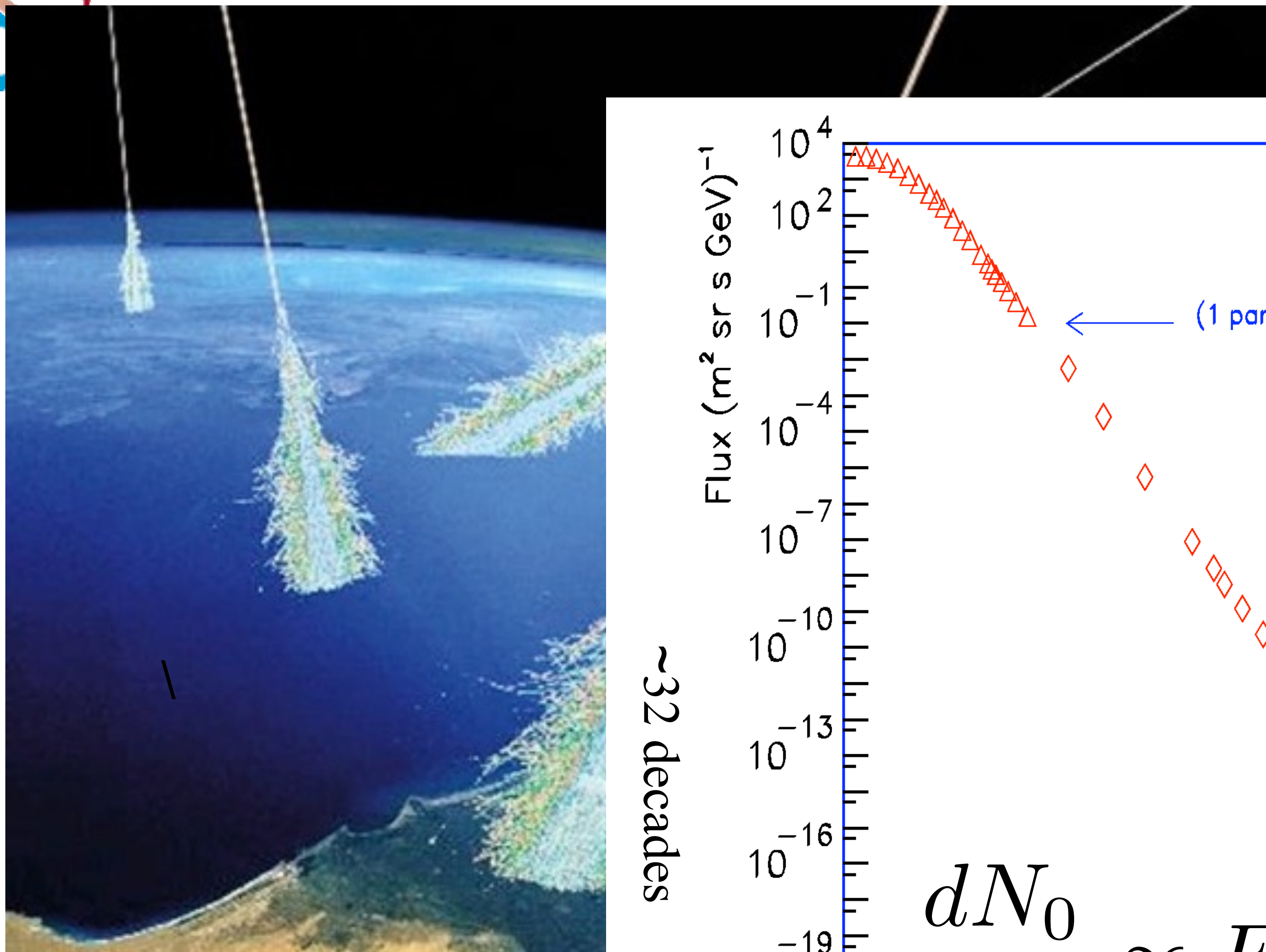

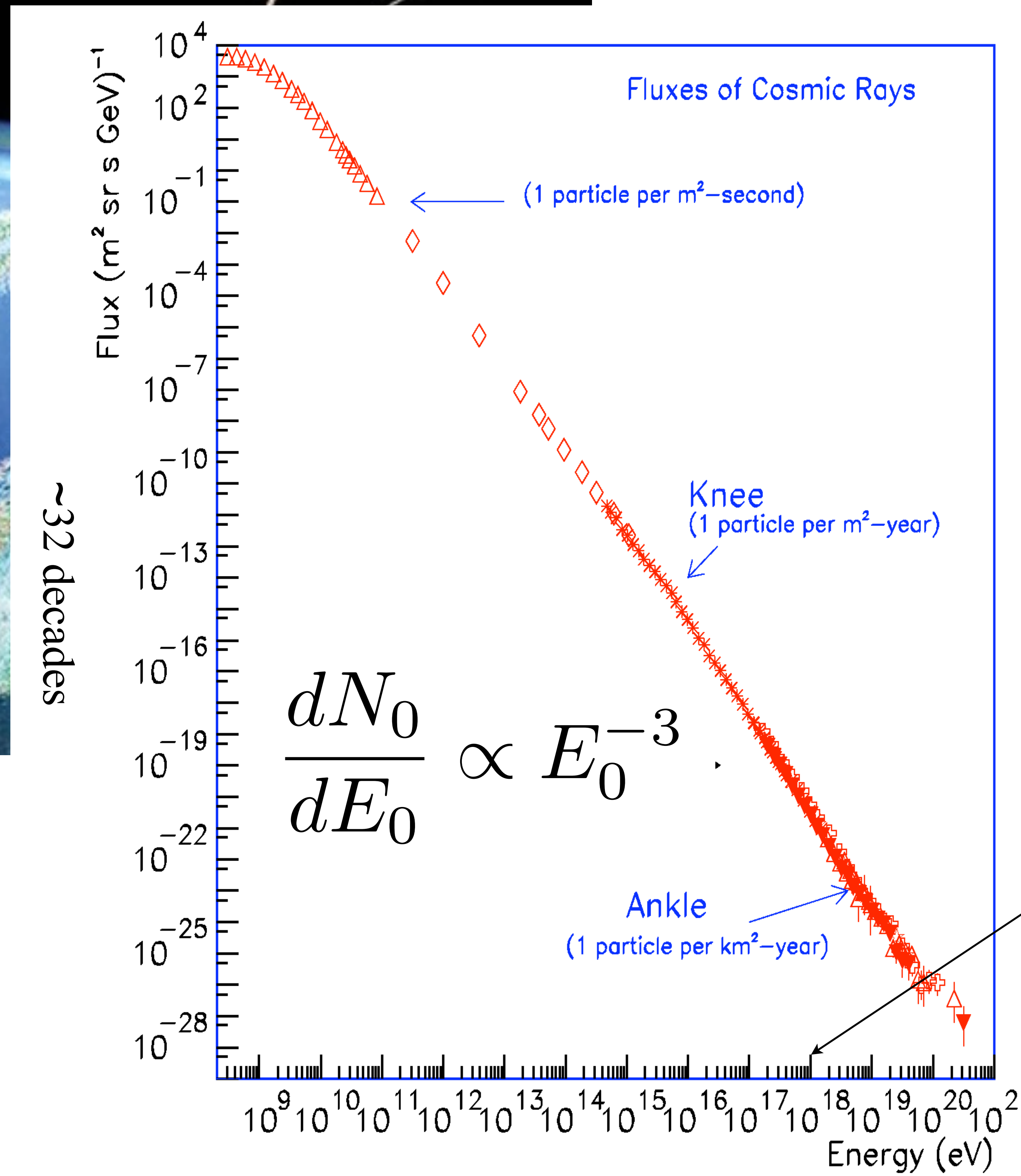

~32 decades

$$\frac{dN_0}{dE_0} \propto E_0^{-3}$$

~12 decades

EeV

TeV: LHC energy

Systematics: atmospheric flux

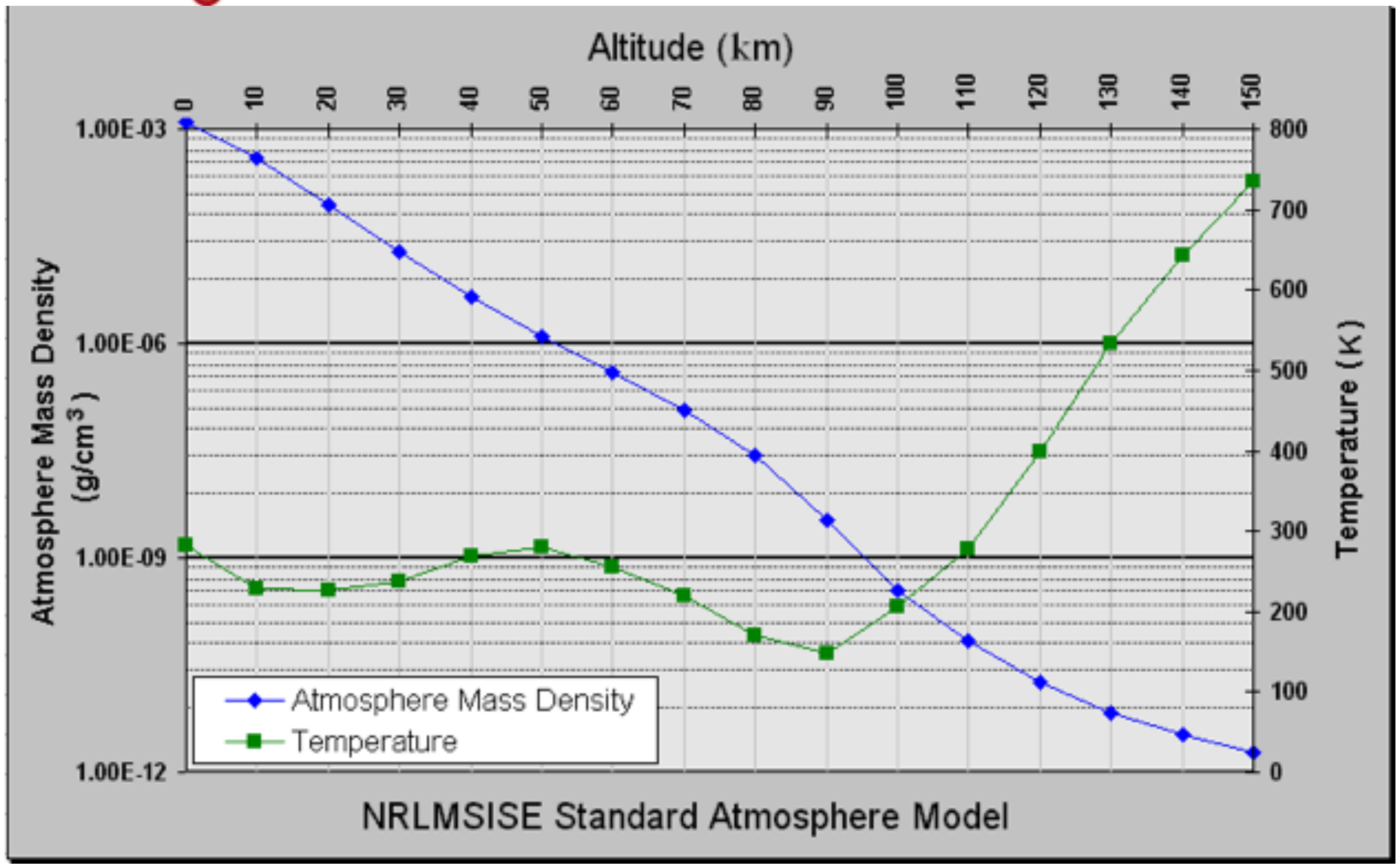

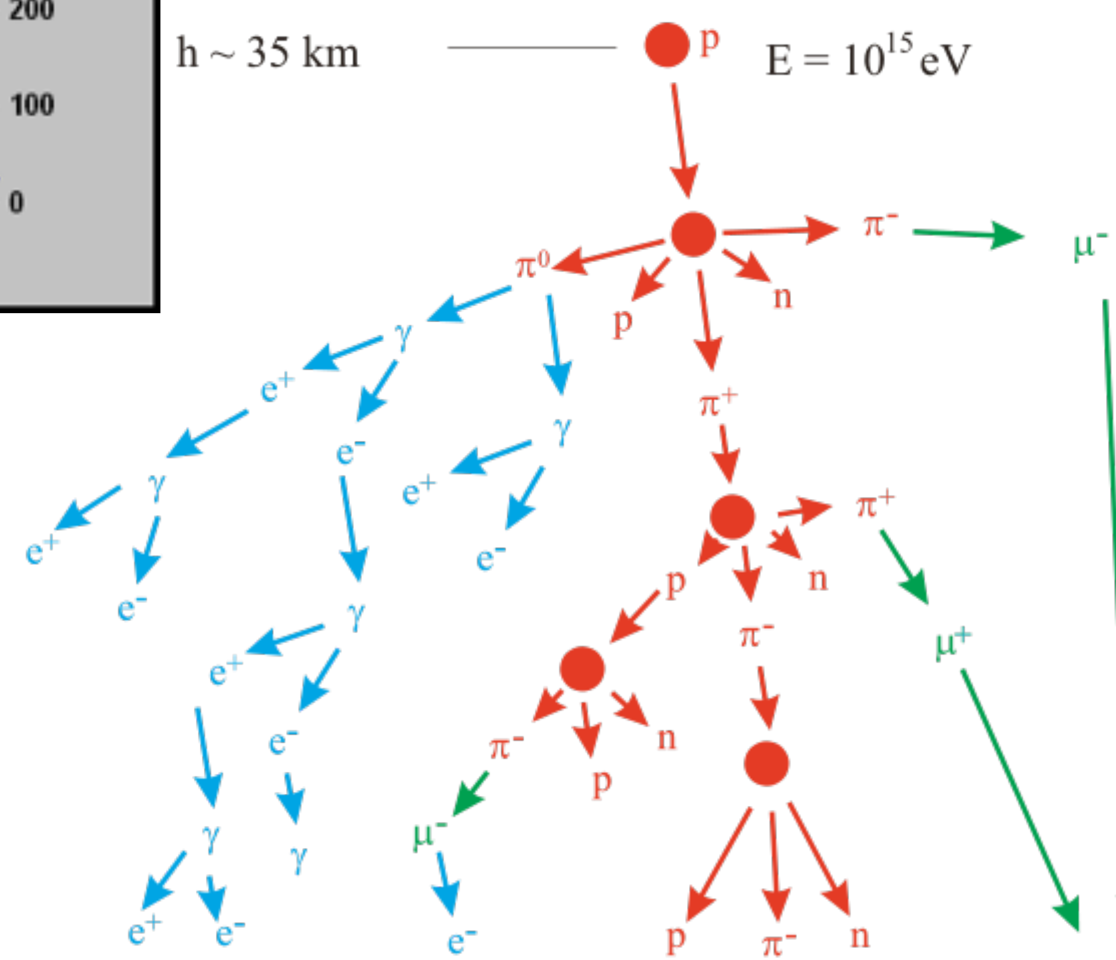

$$\pi^{\pm} \rightarrow \mu^{\pm} \overset{(-)}{\nu}_{\mu} (\sim 100\,\%)$$

$$K^{\pm} \rightarrow \mu^{\pm} \overset{(-)}{\nu}_{\mu} (\sim 63.5\,\%).$$

Systematics: atmospheric flux

Cecchini & Spurio

http://www.geosci-instrum-method-data-syst.net/1/185/2012/gi-1-185-2012.pdf

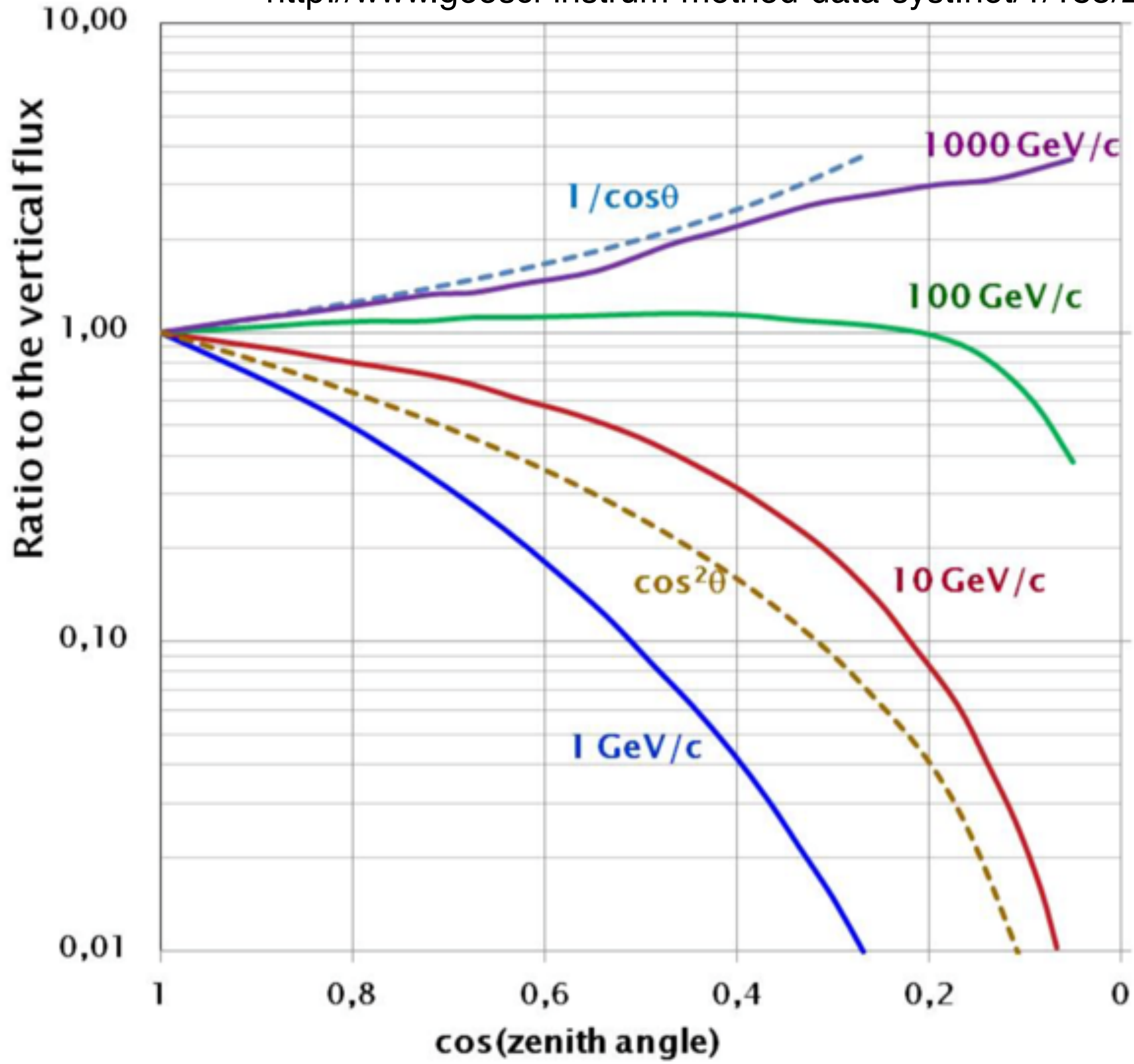

Inverse problem : muon propagation

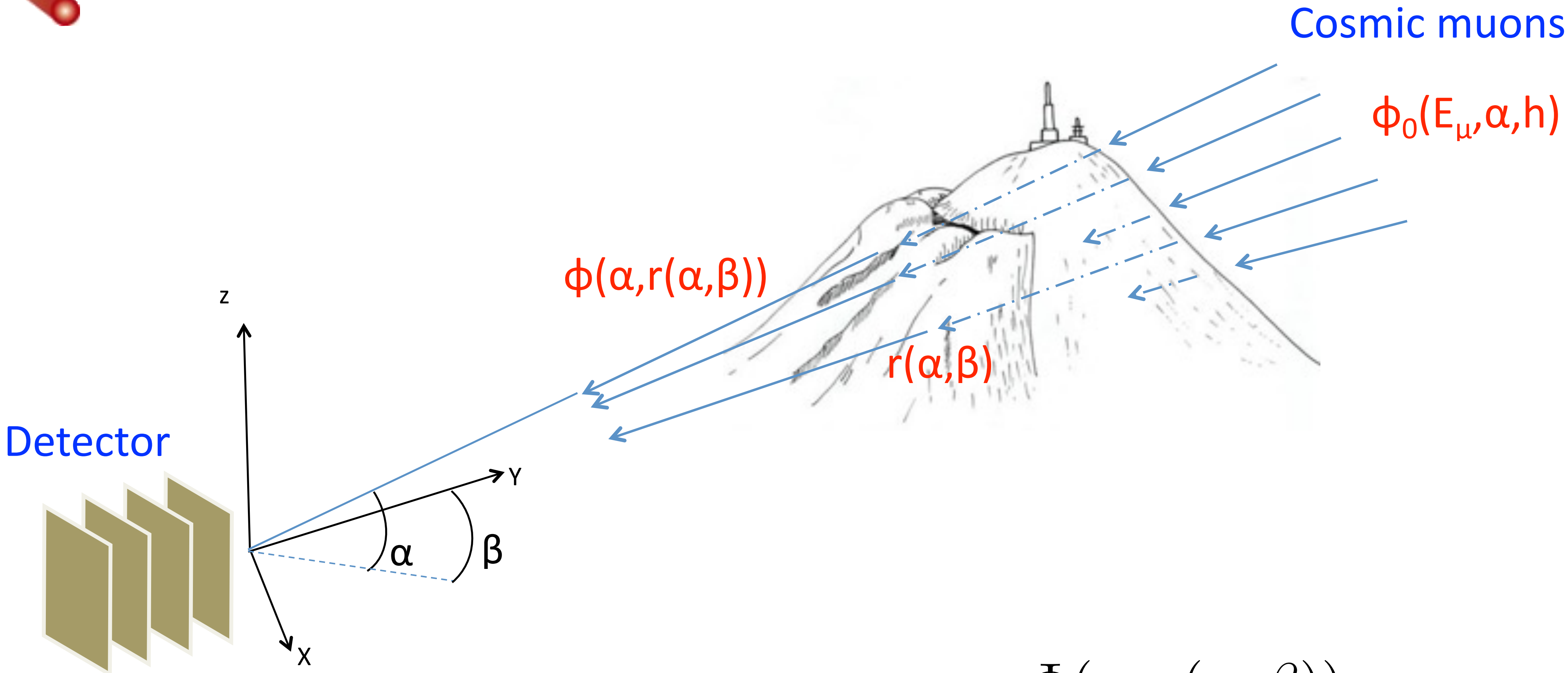

$$\mathcal{T}_{\rho}(\alpha, r(\alpha,\beta)) = \frac{\Phi(\alpha, r(\alpha,\beta))}{\Phi_0(\alpha)}$$

$$\boxed{\int \rho(\alpha,\beta)dr = \mathcal{F}(\mathcal{T}(\alpha,\beta))}$$

Muon energy loss

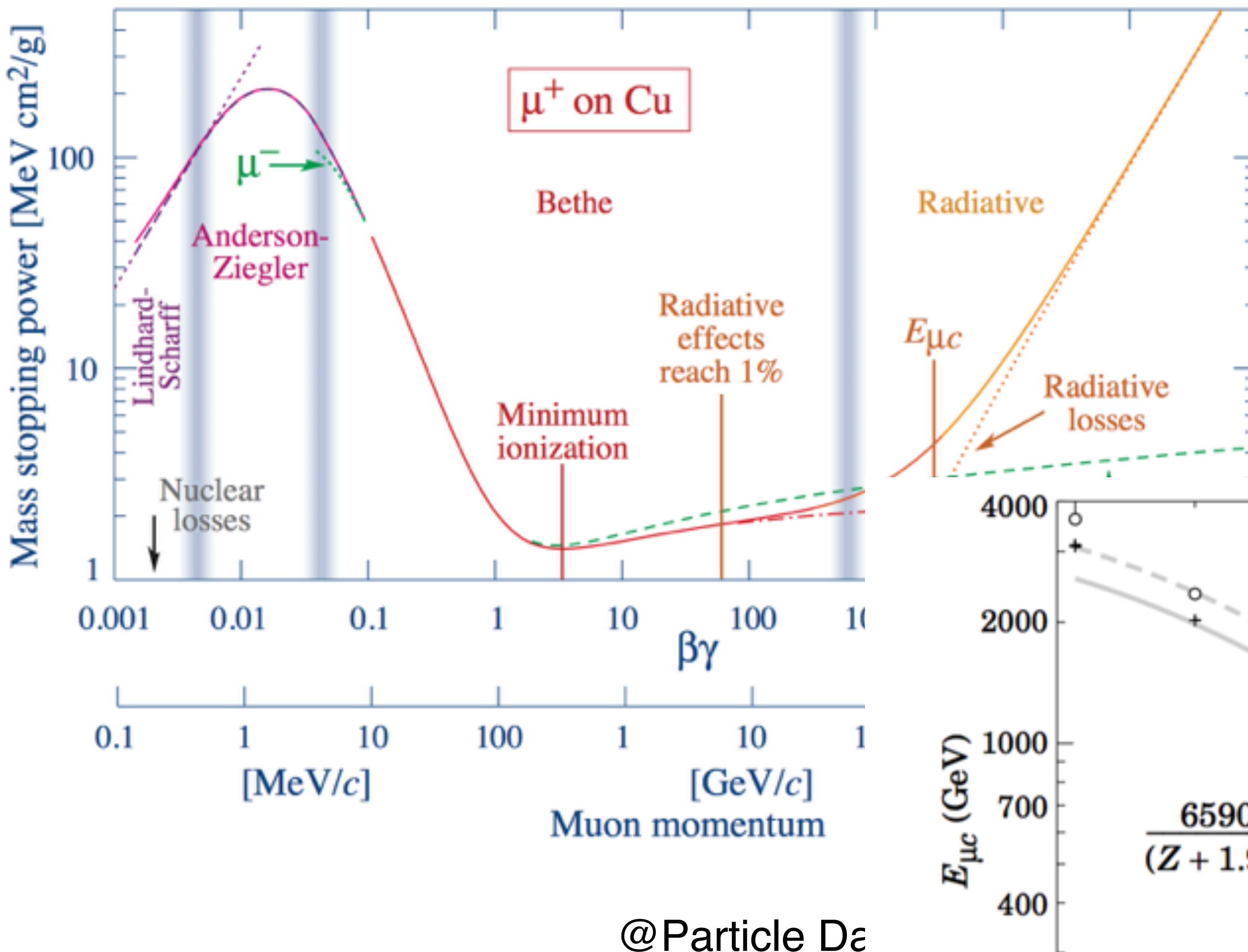

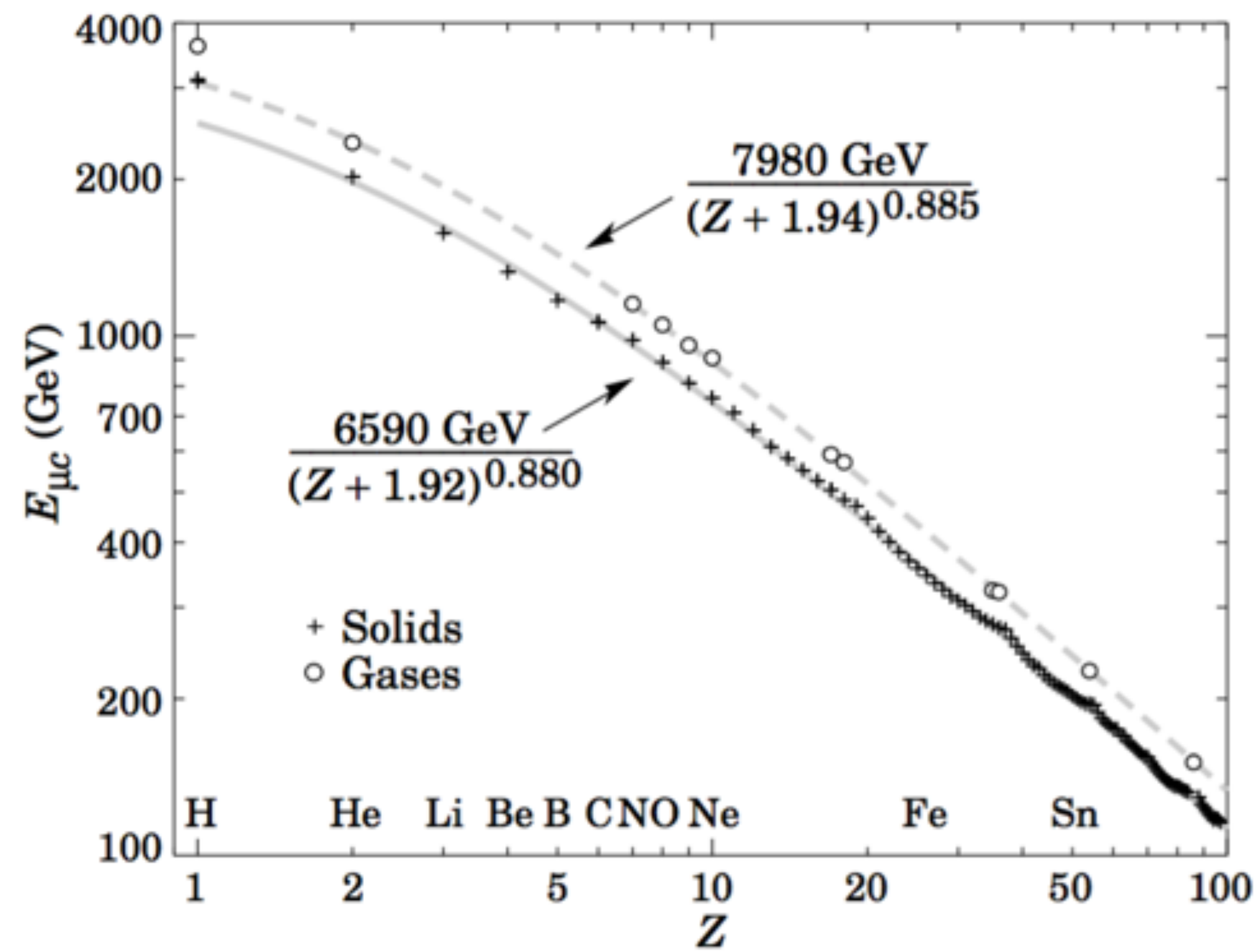

Systematics: muon propagation : energy losses

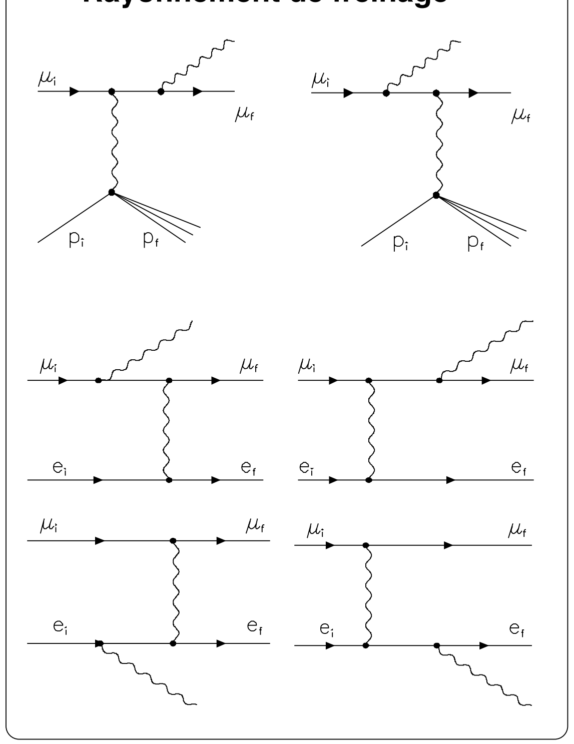

Rayonnement de freinage

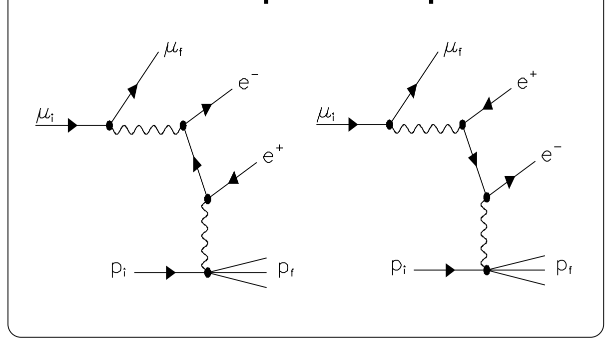

Création de paires de leptons

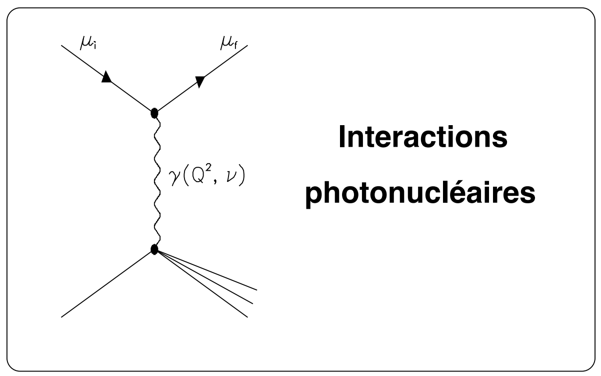

Interactions photonucléaires

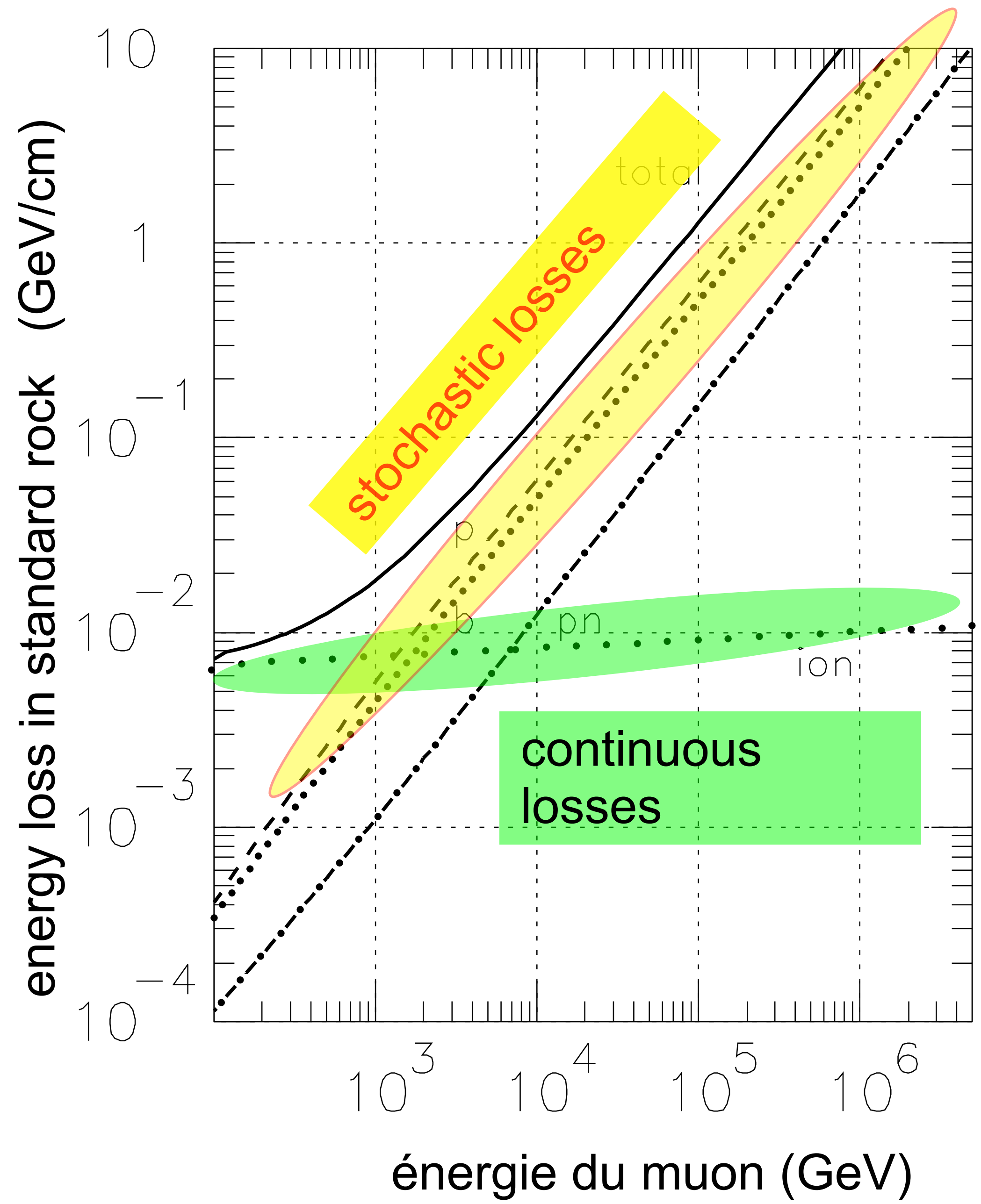

Systematics: muon propagation : energy losses

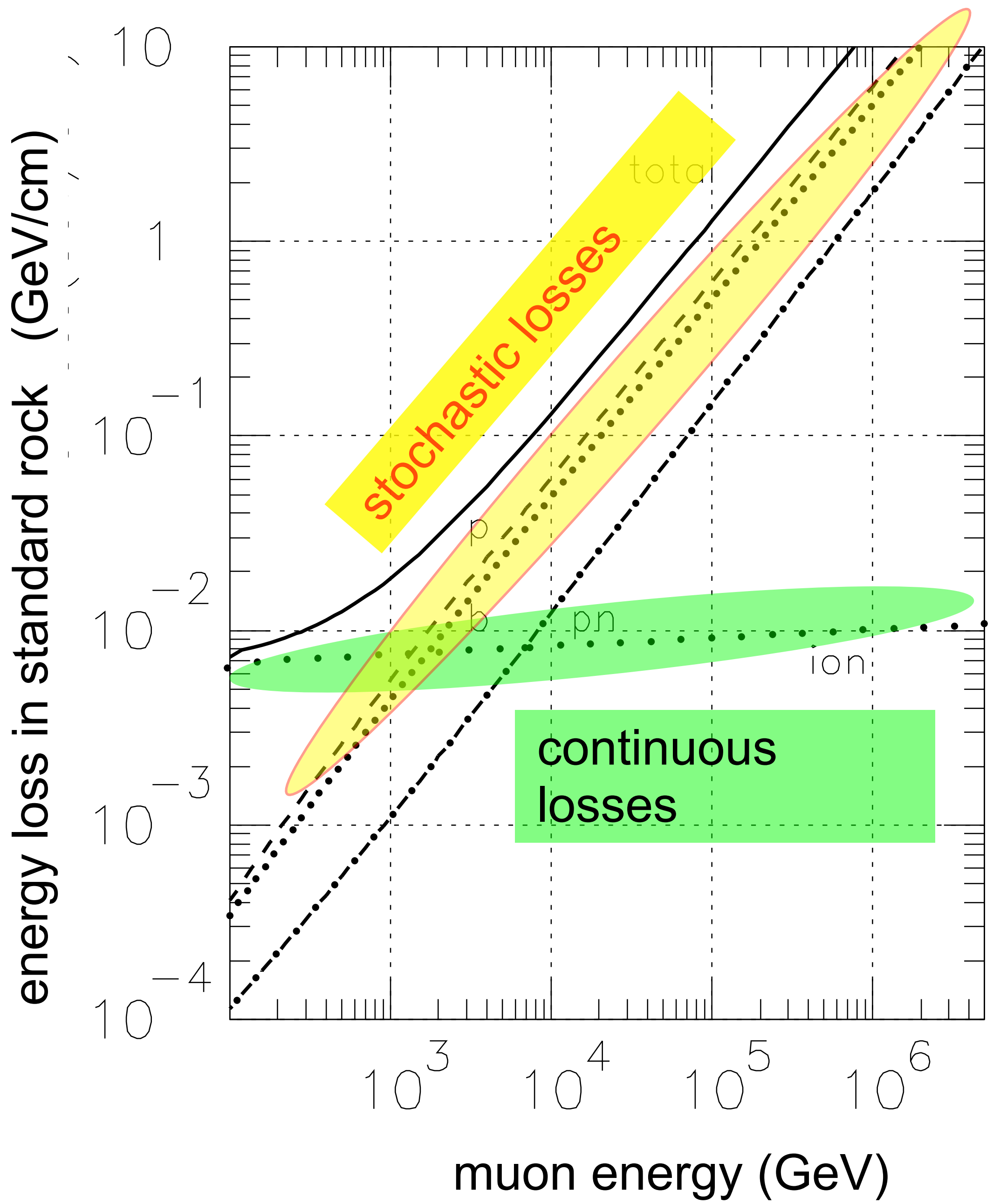

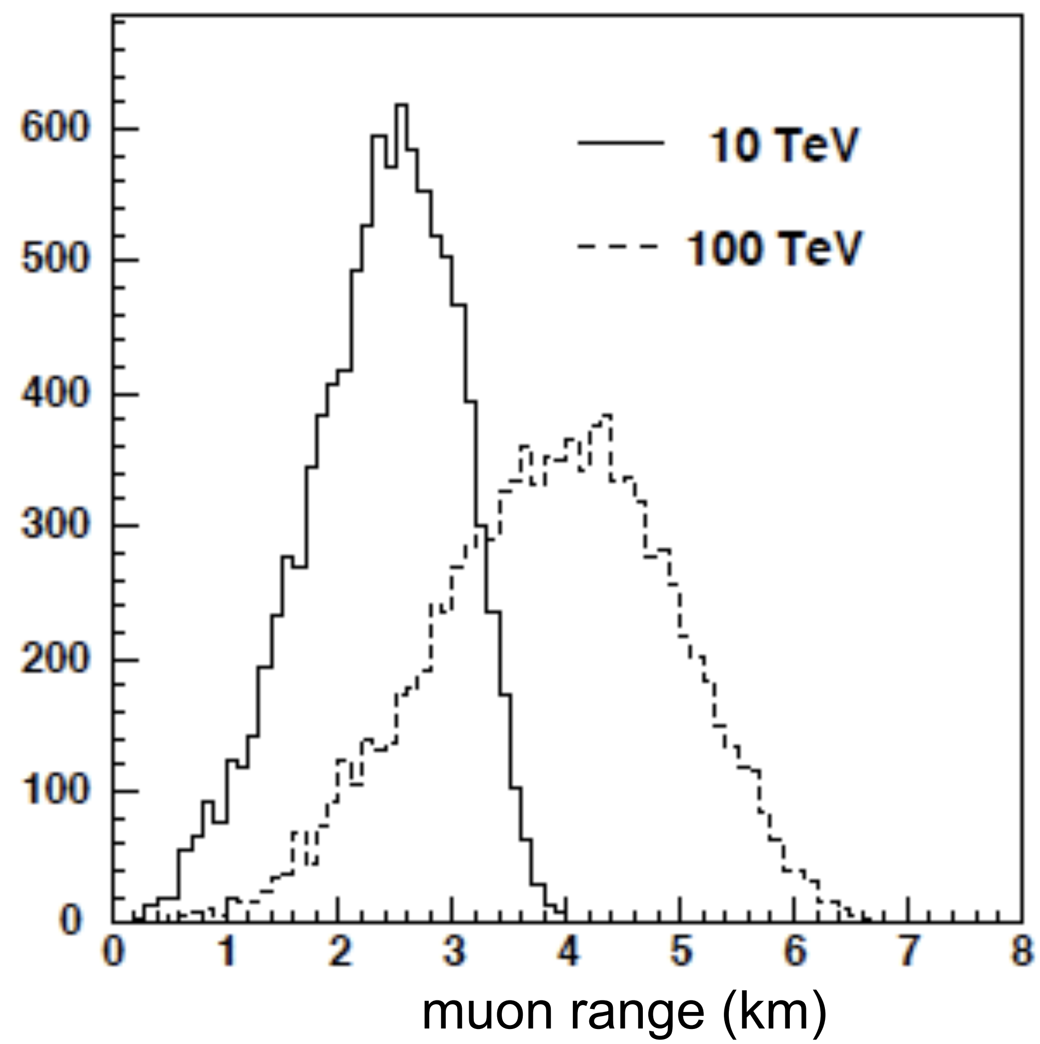

Above TeV, energy losses dominated by stochastic processes
Muon scattering rather low, but dependent on the muon energy

Systematics: muon propagation : energy losses

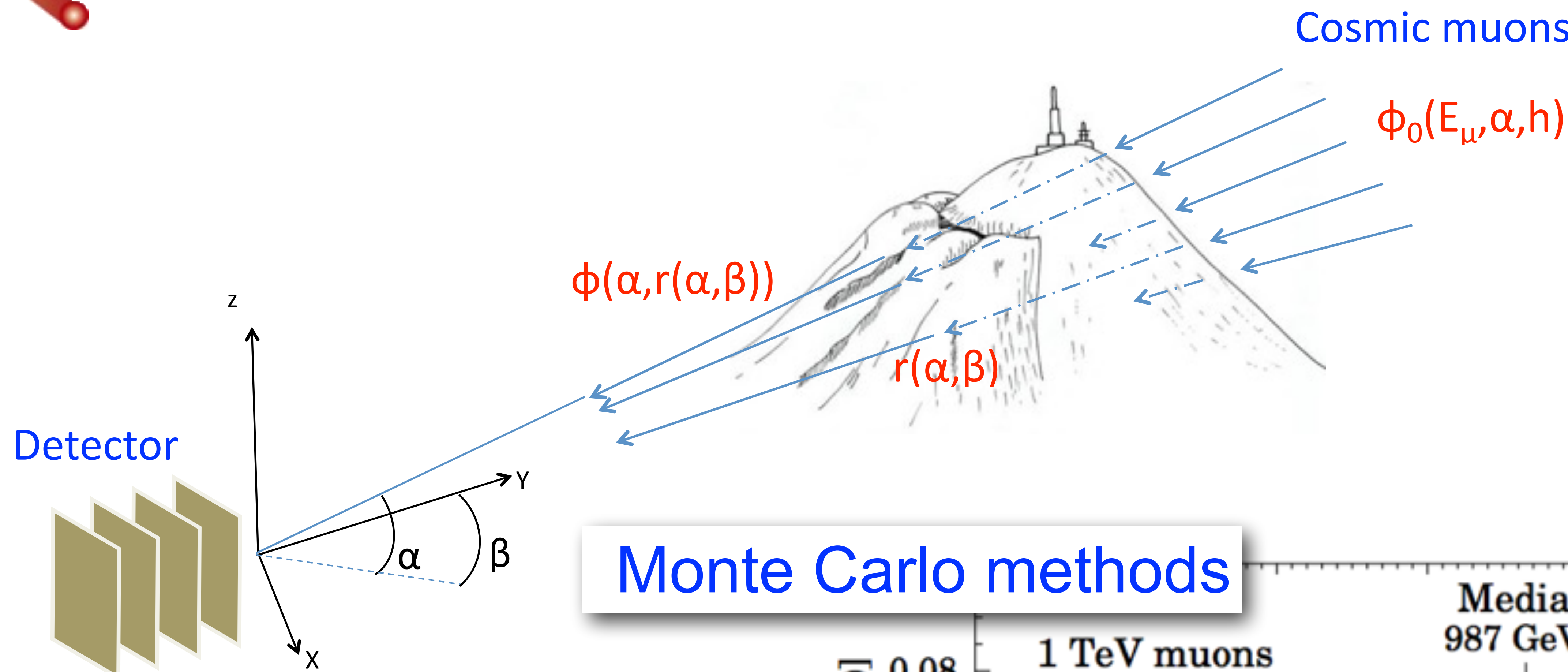

$$N_0(\alpha) = \int_{E_\mu \approx 1GeV}^{\infty} \varphi_0(E_\mu)\,dE_\mu$$

$$N(\alpha,\beta) = \int_{E_{\mu\,\min}}^{\infty} \varphi_0(E_\mu)\,dE_\mu$$

$$E_{\mu\,\min} \propto \int_{R(\alpha,\beta)} \rho(r,\alpha,\beta)\,dr$$

Monte Carlo methods

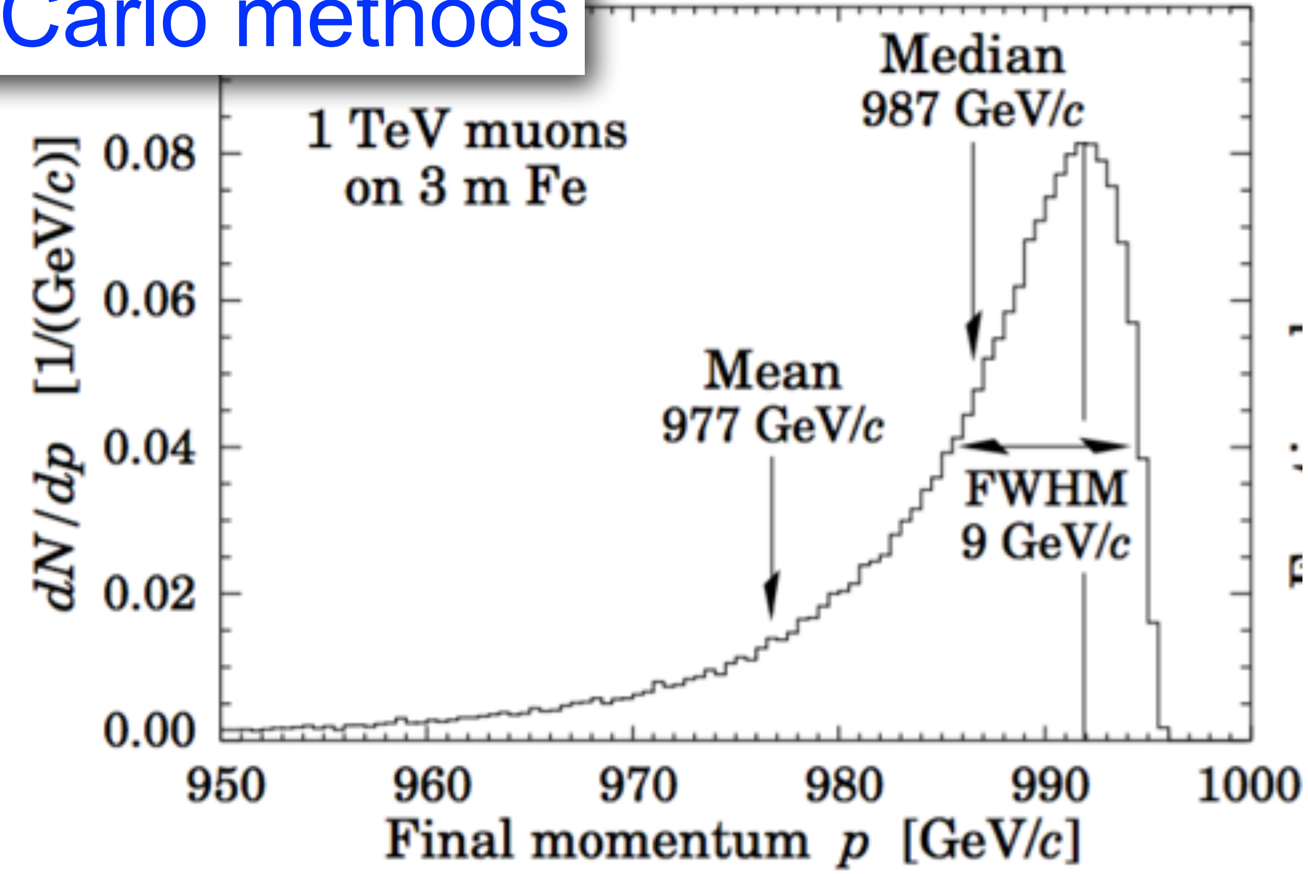

$\boxed{N/N_0\,(\alpha,\beta)} \Longrightarrow \boxed{\int\rho(r,\alpha,\beta)\,dr \,/ \int dr}$

$$\left.\frac{d\sigma}{d\nu}\right|_{\text{brems, nucl}} = \alpha\left(2Z\frac{m_e}{M_\mu}r_e\right)^2\left(\frac{4}{3}-\frac{4}{3}\nu+\nu^2\right)\frac{\Phi(\delta)}{\nu}$$

$$b_{\text{pair, nucl}} = -\frac{1}{E}\left.\frac{dE}{dx}\right|_{\text{pair, nucl}} = \frac{N_A}{A}\int_0^1 \nu\frac{d\sigma}{d\nu}d\nu$$

$$b_{\text{pair, elec}} = -\frac{1}{E}\left.\frac{dE}{dx}\right|_{\text{pair, elec}} = \frac{Z}{A}\left(0.073\ \ln\left(\frac{2E/M_\mu}{1+g\,Z^{2/3}E/M_\mu}\right)-0.31\right)\times 10^{-6}\text{cm}^2/\text{g}$$

Transmission muography in a nutshell ...

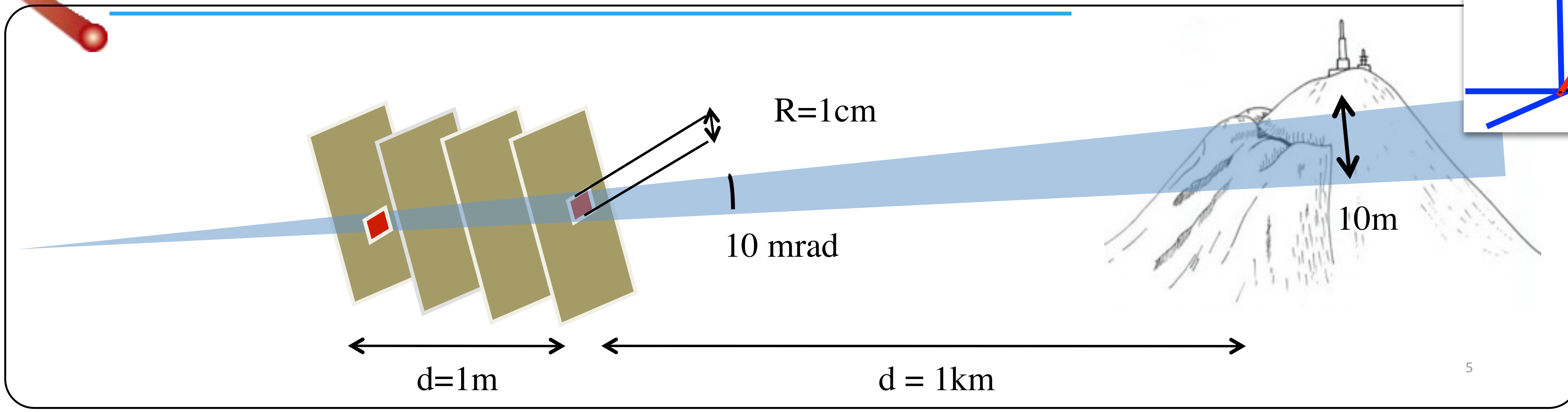

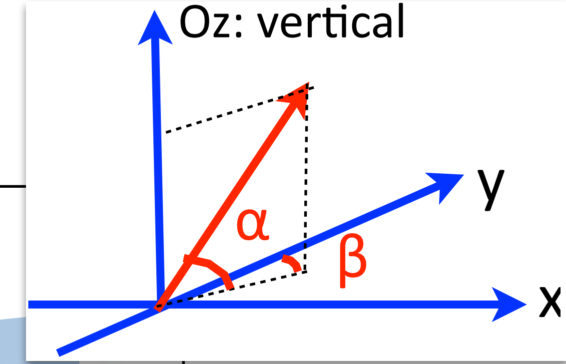

$$\mathcal{T}_\rho(\alpha, r(\alpha,\beta)) = \frac{\Phi(\alpha, r(\alpha,\beta))}{\Phi_0(\alpha)}$$

$$\boxed{\int \rho(\alpha,\beta)dr = \mathcal{F}(\mathcal{T}(\alpha,\beta))}$$

$$\Phi(\alpha,\beta) = \frac{N(\alpha,\beta)}{Seff(\alpha,\beta)\Delta T \Delta\Omega}$$

$$S_{eff} = S_{det}\varepsilon_{det}\varepsilon_{geom}\varepsilon_{illum}$$

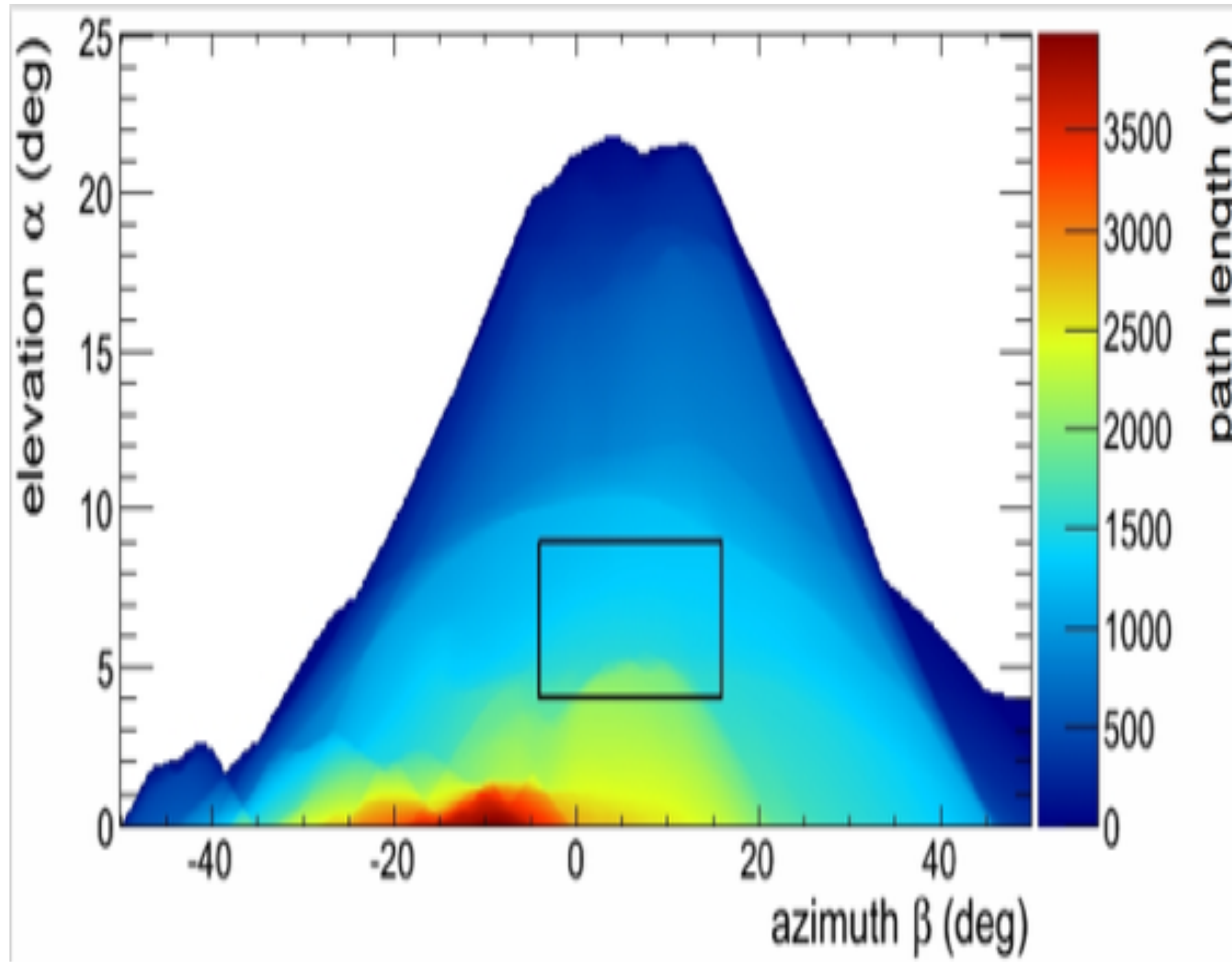

Transmission muography in a nutshell ...

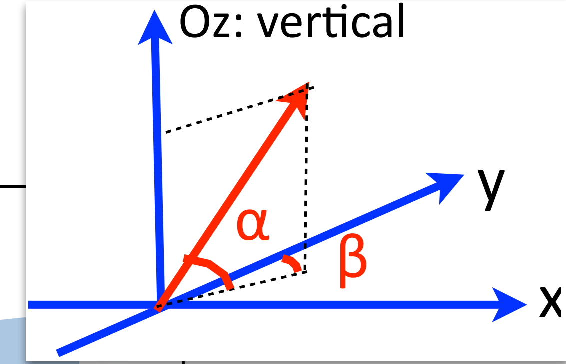

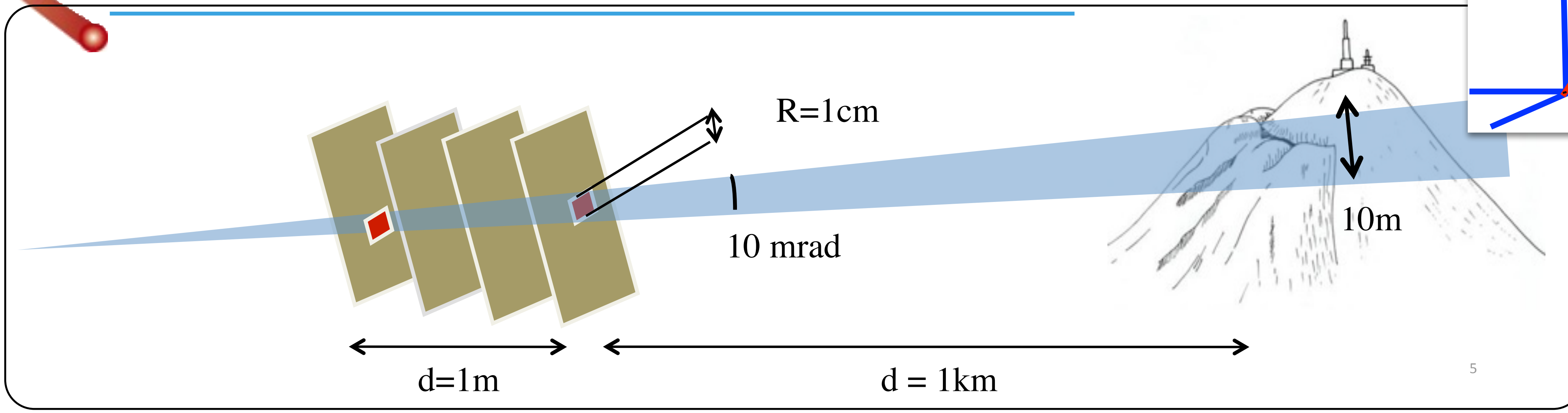

$$\mathcal{T}_\rho(\alpha, r(\alpha,\beta)) = \frac{\Phi(\alpha, r(\alpha,\beta))}{\Phi_0(\alpha)}$$

$$\boxed{\int \rho(\alpha,\beta)dr = \mathcal{F}(\mathcal{T}(\alpha,\beta))}$$

$$\Phi(\alpha,\beta) = \frac{N(\alpha,\beta)}{Seff(\alpha,\beta)\Delta T \Delta\Omega}$$

$$S_{eff} = S_{det}\varepsilon_{det}\varepsilon_{geom}\varepsilon_{illum}$$

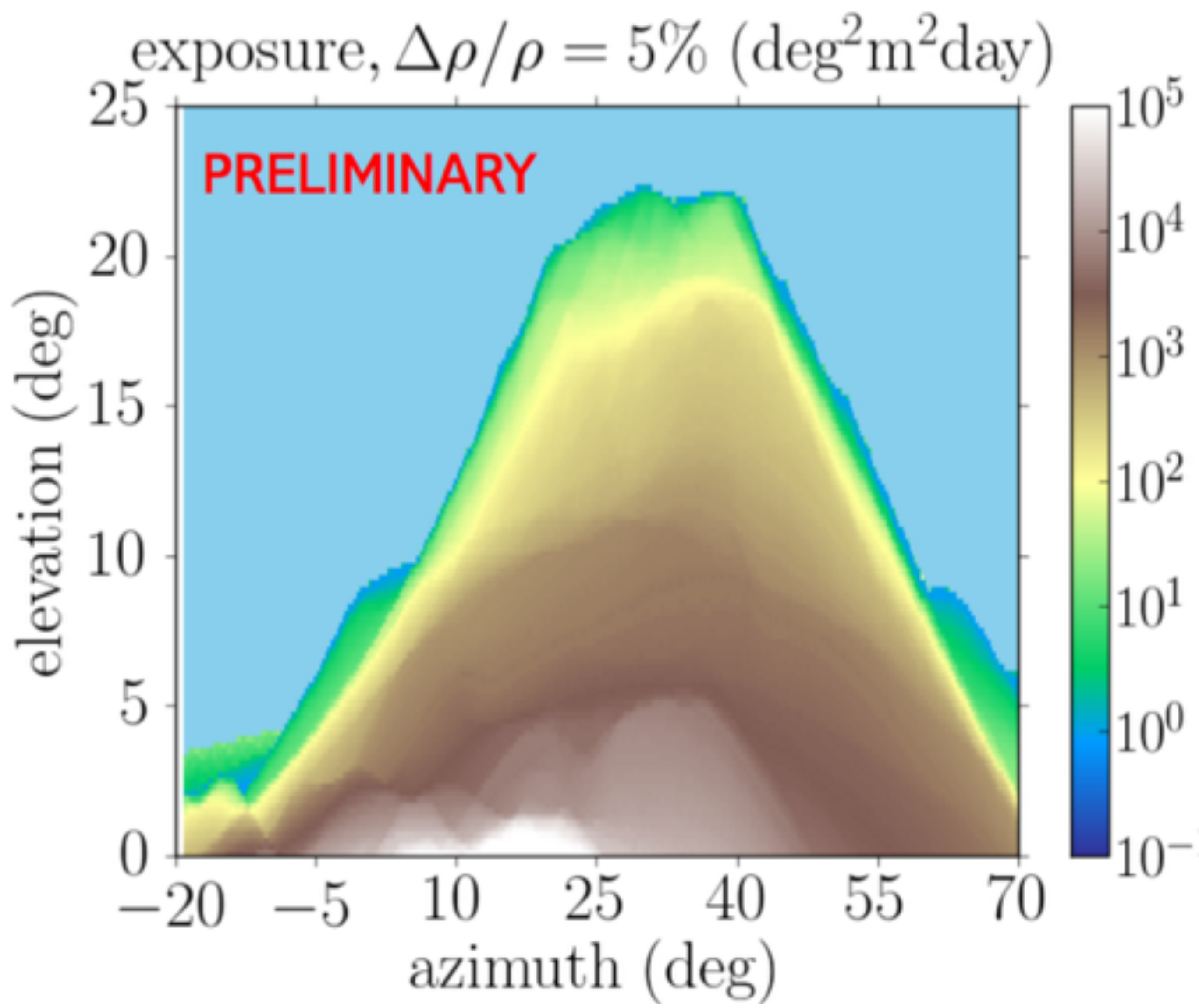

Crosscheck for a uniform volcano with ρ=1.8g/cm3

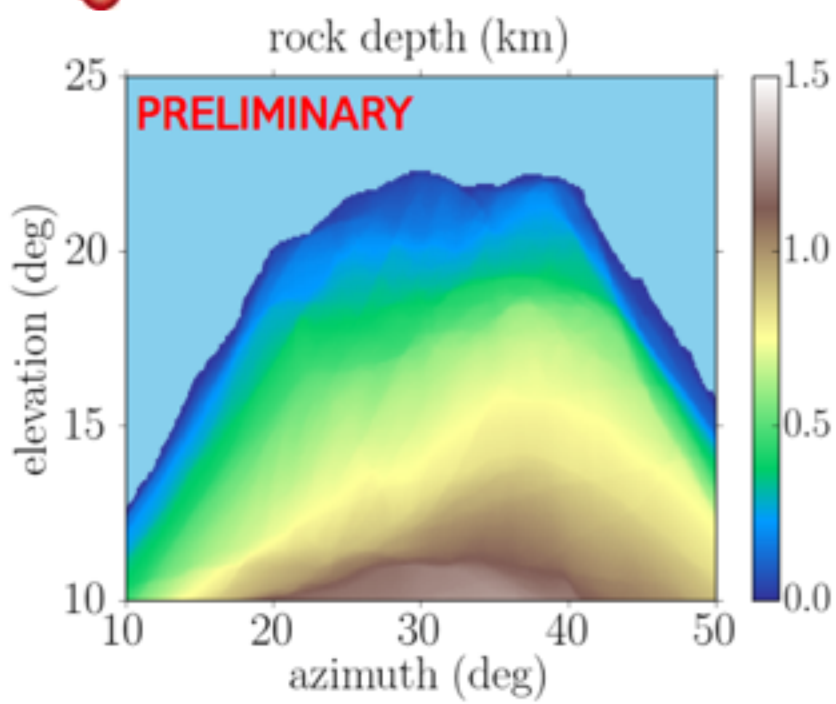

- The bias is negligible, $\sim$ 10-20 mg/cm^3, except close to the rock border, where the transmitted and free sky flux mix.
- Few degrees farther from the border the statistical uncertainties are below $\sim$ 100 mg/cm^3.

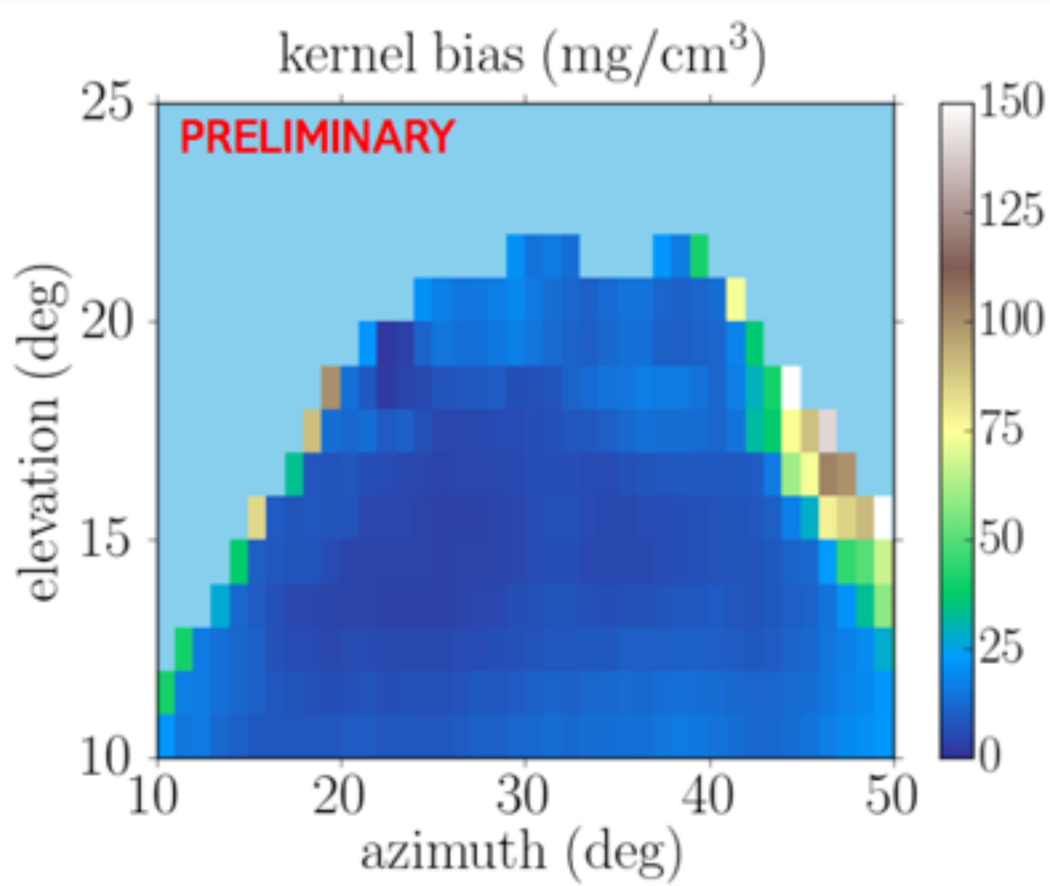

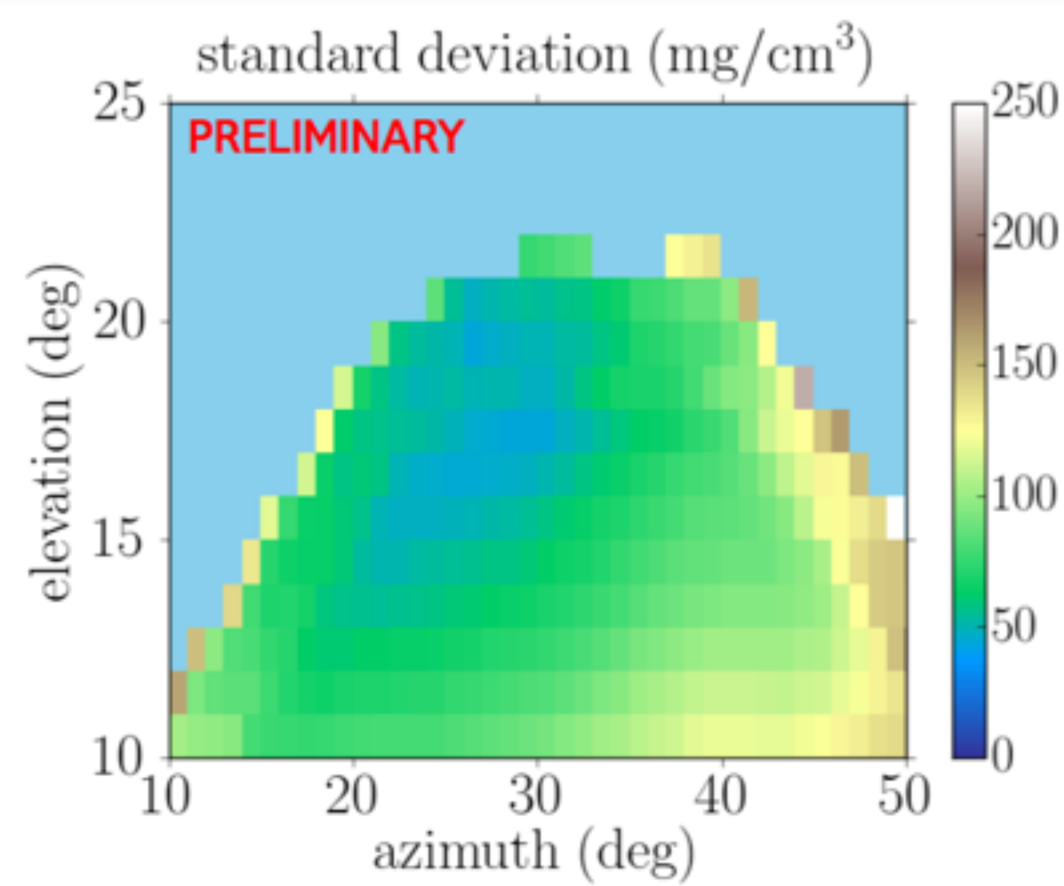

Crosscheck for a non-uniform volcano

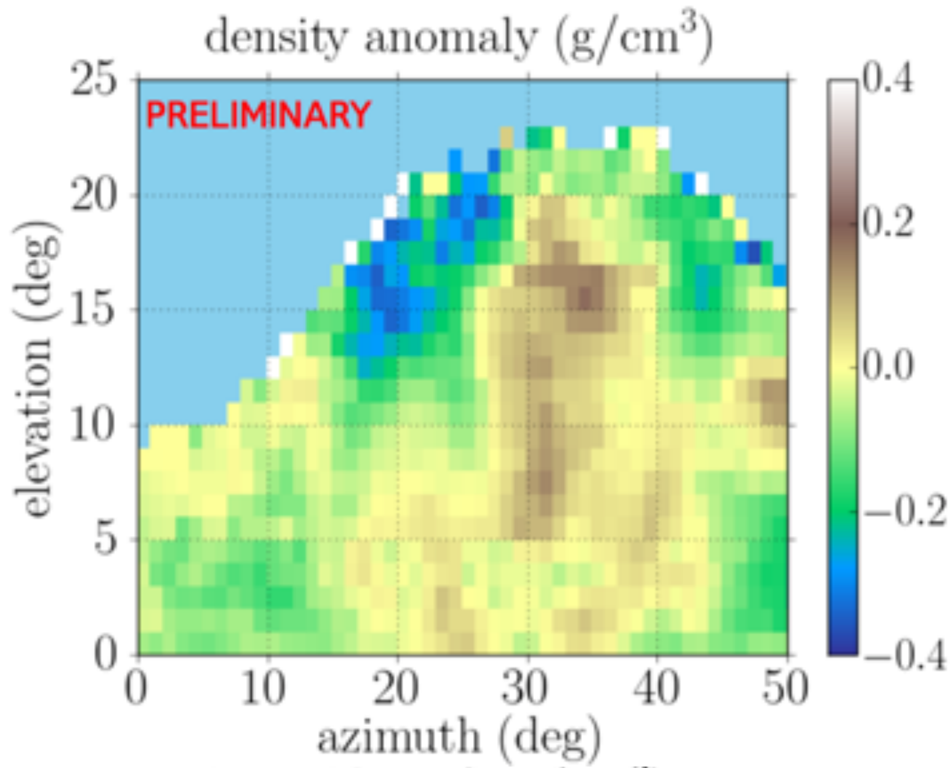

- The bias is mostly the difference between the true and blurred images of density. It is below 100 mg/cm^3 beneath a few degrees from the border.
- The statistical uncertainties are comparable to the uniform case, 50-100 mg/cm^3.